

Evolution of the Color-Magnitude Relation in High-Redshift Clusters: Blue Early-Type Galaxies and Red Pairs in RDCS J0910+5422

S. Mei¹, J. P. Blakeslee¹, S. A. Stanford^{2,3}, B. P. Holden⁴, P. Rosati⁶, V. Strazzullo^{20,6}, N. Homeier¹, M. Postman^{1,5}, M. Franx¹², A. Rettura⁶, H. Ford¹, G. D. Illingworth⁴, S. Etti¹⁹, R.J. Bouwens⁴, R. Demarco¹, A.R. Martel¹, M. Clampin⁵, G.F. Hartig⁵, P. Eisenhardt⁷, D.R. Ardila¹, F. Bartko⁸, N. Benítez¹⁸, L.D. Bradley¹, T.J. Broadhurst⁹, R.A. Brown⁵, C.J. Burrows⁵, E.S. Cheng¹⁰, N.J.G. Cross¹⁷, P.D. Feldman¹, D.A. Golimowski¹, T. Goto¹, C. Gronwall¹³, L. Infante¹⁴, R.A. Kimble¹¹, J.E. Krist⁵, M.P. Lesser¹⁵, F. Menanteau¹, G.R. Meurer¹, G.K. Miley¹², V. Motta¹⁴, M. Sirianni⁵, W.B. Sparks⁵, H.D. Tran¹⁶, Z.I. Tsvetanov¹, R.L. White⁵, & W. Zheng¹

ABSTRACT

The color-magnitude relation has been determined for the RDCS J0910+5422 cluster of galaxies at redshift $z = 1.106$. Cluster members were selected from HST Advanced Camera for Surveys (ACS) images, combined with ground-based near-IR imaging and optical spectroscopy. Postman et al. (2005) morphological classifications were used to identify the early-type galaxies.

The observed early-type color-magnitude relation (CMR) in $(i_{775} - z_{850})$ versus z_{850} shows an intrinsic scatter in color of 0.060 ± 0.009 mag, within $1'$ from the cluster X-ray emission center. Both the ellipticals and the S0s show small scatter about the CMR of 0.042 ± 0.010 mag and 0.044 ± 0.020 mag, respectively. From the scatter about the CMR, a mean luminosity-weighted age $\bar{t} > 3.3$ Gyr ($z_f > 3$) is derived for the elliptical galaxies, assuming a simple stellar population modeling (single burst solar metallicity). This is consistent with a previous study of the cluster RDCS 1252.9-292 at $z=1.24$ (Blakeslee et al.).

Strikingly, the S0 galaxies in RDCS J0910+5422 are systematically bluer in $(i_{775} - z_{850})$ by 0.07 ± 0.02 mag, with respect to the ellipticals. The blue S0s are predominantly elongated in shape; the distribution of their ellipticities is inconsistent with a population of axisymmetric disk galaxies viewed at random orientations, suggesting either that they are intrinsically prolate or there is some orientation bias in the S0 classification. The ellipticity distribution as a function of color indicates that the face-on S0s in this particular cluster have likely been classified as elliptical. Thus, if anything, the offset in color between the elliptical and S0 populations may be even more significant.

The color offset between S0 and E corresponds to an age difference of ≈ 1 Gyr, for a single-burst solar metallicity model. Alternatively, it could be the result of a different star formation history; a solar metallicity model with an exponential decay in star formation will reproduce the offset for an age of 3.5 Gyr, i.e. the S0s have evolved gradually from star forming progenitors. The color offset could also be reproduced by a factor of ~ 2 difference in metallicity, but the two populations would each need to have very small scatter in metallicity to reproduce the small scatter in color.

The early-type population in this cluster appears to be still forming. The blue early-type disk galaxies in RDCS J0910+5422 likely represent the direct progenitors of the more evolved S0s that follow the same red sequence as ellipticals in other clusters.

Thirteen red galaxy pairs are observed and the galaxies associated in pairs constitute $\sim 40\%$ of the CMR galaxies in this cluster. This finding is consistent with the conclusions of van Dokkum and Tran et al. that most of the early-type galaxies grew from passive red mergers.

Subject headings: galaxies: clusters: individual (RDCS J0910+5422) – galaxies: elliptical and lenticular – galaxies: evolution

1. Introduction

The Advanced Camera for Surveys (ACS; Ford et al. 2002), by virtue of its high spatial resolution and sensitivity, allows us to study galaxy clusters in great detail up to redshifts of unity and beyond. At these redshifts, galaxy clusters are still assembling and galaxies are evolving towards the populations that we observe today. Recent results from our ACS Intermediate Redshift Cluster Survey (Blakeslee et al. 2003a; Lidman et al. 2004; Demarco et al. 2005; Goto et al. 2005; Holden et al. 2005a; Holden et al. 2005b; Homier et al. 2005; Postman et al. 2005) have shown that galaxy clusters at redshift around unity show

many similarities with local clusters, in terms of galaxy populations and their distribution, but also significant differences in galaxy morphology, ellipticity, and mass–luminosity ratios. The strongest evolution observed in the early–type population is a deficit of a S0 population in this sample when compared to lower redshift samples (Postman et al. 2005). This would give evidence that the formation of the S0 population is still under way in clusters at redshift unity.

One of the most striking similarities is that the tight relation between early-type galaxy colors and luminosities that applies locally (the color–magnitude relation; CMR) is already in place at redshifts as high as $z \sim 1.3$ (e.g. Stanford et al. 1997; Mullis et al. 2005). The CMR in local samples of galaxy clusters presents universal properties, in terms of scatter and zero point (Bower et al. 1992; van Dokkum et al. 1998, Hogg et al. 2004; López–Cruz et al. 2004; Bell et al. 2004; Bernardi et al. 2005; McIntosh et al. 2005) that evolve back in time in agreement with passively evolving models (Ellis et al. 1997; Stanford, Eisenhardt, & Dickinson 1998; van Dokkum et al. 2000, 2001; Blakeslee et al. 2003a; Holden et al. 2004; De Lucia et al. 2004; Blakeslee et al. 2005). ACS enables accurate measurement of the scatter around the CMR, with enough precision to seriously constrain galaxy formation age, which is impossible to obtain from ground–based data (see for example Holden et al. 2004). The measurement of the CMR scatter of the first cluster in our ACS cluster survey, RXJ1252.9-292, permitted us to constrain the mean luminosity–weighted age for the ellipticals to be > 2.6 Gyr ($z > 2.7$) (Blakeslee et al. 2003a), based on simple modeling. In this paper, we extend the results obtained in Blakeslee et al. (2003a) to RXJ 0910+5422.

RXJ 0910+5422 is part of the ACS cluster survey (guaranteed time observation, GTO, program #9919), that includes eight clusters in the redshift range at $0.8 < z < 1.3$, selected in the X–ray, optical and near–IR (Ford et al. 2004). RXJ 0910+5422 was selected from the ROSAT Deep Cluster Survey (Rosati et al. 1998) and confirmed with near–IR and spectroscopic observations by Stanford et al. (2002). Extensive followup spectroscopy at the Keck Observatory has been carried out in a magnitude limited sample reaching $K_s = 20.0$ mag in the central 3 arcmin (Stanford et

¹Dept. of Physics & Astronomy, Johns Hopkins University, Baltimore, MD 21218; smeij@pha.jhu.edu

²Department of Physics, University of California, Davis, CA 94516

³Institute of Geophysics and Planetary Physics, Lawrence Livermore National Lab, Livermore, CA 94551

⁴Lick Observatory, University of California, Santa Cruz, CA 95064

⁵Space Telescope Science Institute, 3700 San Martin Drive, Baltimore, MD 21218

⁶European Southern Observatory, Karl-Schwarzschild-Str. 2, D-85748 Garching, Germany

⁷Jet Propulsion Laboratory, CalTech, 4800 Oak Grove Drive, Pasadena, CA 91125

⁸Bartko Science & Technology, 14520 Akron Street, Brighton, CO 80602.

⁹School of Physics and Astronomy, Tel Aviv University, Tel Aviv 69978, Israel

¹⁰Conceptual Analytics, LLC, 8209 Woburn Abbey Road, Glenn Dale, MD 20769.

¹¹NASA Goddard Space Flight Center, Code 681, Greenbelt, MD 20771.

¹²Leiden Observatory, Postbus 9513, 2300 RA Leiden, Netherlands.

¹³Dept. of Astronomy & Astrophysics, Penn State University, University Park, PA 16802.

¹⁴Dept. de Astronomía y Astrofísica, Pontificia Universidad Católica, Casilla 306, Santiago 22, Chile.

¹⁵Steward Observatory, University of Arizona, Tucson, AZ 85721.

¹⁶W. M. Keck Observatory, 65-1120 Mamalahoa Hwy., Kamuela, HI 96743

¹⁷Royal Observatory Edinburgh, Blackford Hill, Edinburgh, EH9 3HJ, UK

¹⁸Instituto de Astrofísica de Andalucía (CSIC), Camino Bajo de Huétor 50, Granada 18008, Spain

¹⁹INAF - Osservatorio Astronomico, via Ranzani 1, 40127 Bologna, Italy

²⁰Dipartimento di Scienze Fisiche, Università Federico II, I-80126 Napoli, Italy

al. 2005; in preparation). The mean redshift of the cluster was measured to be $z = 1.106$ (Stanford et al. 2002). In this paper, we combine ACS imaging with ground-based spectroscopy and near-IR imaging to constrain galaxy ages and formation histories from the study of their color-magnitude relation. We discuss the properties of the elliptical (E) and lenticular (S0) populations separately in the light of simple galaxy formation scenarios.

2. Observations

RXJ 0910+5422 was observed in March 2004 with the ACS WFC (Wide Field Camera) in the F775W (i_{775}) and F850LP (z_{850}) bandpasses, with total exposure times of 6840 s and 11440 s, respectively. The ACS WFC scale is $0.05''/\text{pixel}$, and its field of view is $210'' \times 204''$. The APSIS pipeline (Blakeslee et al. 2003b), with a *Lanczos3* interpolation kernel, was used for processing the images. The ACS photometric zero-points (AB system) are 25.654 mag and 24.862 mag in i_{775} and z_{850} , respectively (Sirrianni et al. 2005). A Galactic reddening of $E(B - V) = 0.019$ towards RXJ 0910+5422 was adopted (Schlegel et al. 1998), with $A_{i_{775}} = 0.039$ and $A_{z_{850}} = 0.029$ (Sirrianni et al. 2005). The ACS WFC field covers an area that at the redshift of this cluster, $z = 1.106$, corresponds to $\approx 1Mpc^2$ in the WMAP cosmology (Spergel et al. 2003): $\Omega_m = 0.27$, $\Omega_\Lambda = 0.73$, $h = 0.71$, adopted as our standard cosmology hereafter). Fig. 1 shows the ACS color image with X-ray contours from Chandra ACIS (Advanced CCD Imaging Spectrometer) data that have been adaptively smoothed (Stanford et al. 2002). Near-IR JK_s and optical i -band images were obtained at Palomar Observatory as described in detail by Stanford et al. (2002).

Optical spectroscopy of galaxies in RXJ 0910+5422 was obtained using the Low Resolution Imaging Spectrometer (LRIS; Oke et al. 1995) on the Keck 1 and 2 telescopes (Stanford et al. 2005; in preparation). Our typical errors in redshift correspond to errors in velocity between 100 and 300 km/s. Objects for spectroscopy were chosen initially from the catalog of objects with $K_s < 20.0$ mag (Vega magnitudes) within the IR imaging area; outside of this area objects were chosen with $i > 21$ mag from the i -band image to fill out masks. Our final sample

included 66% of the objects with $K_s < 20.0$ mag. Spectra were obtained using the 400 lines mm^{-1} grating for all runs except for the initial two discovery masks as reported in Stanford et al. (2002). Nine more masks were observed using LRIS during four runs between January 2001 and February 2003. Usually each mask was observed in a series of four 1800 s exposures, with small spatial offsets along the long axis of the slits. On average, the seeing was $0.9''$. The blue side data were generally not used since the rest frame wavelengths probed at $z = 1.1$ fall far to the blue of the spectral features of interest for galaxies in the cluster. In total, 149 redshifts were obtained.

The slit mask data were separated into slitlet spectra and then reduced using standard long-slit techniques. A fringe frame was constructed for each exposure from neighboring exposures, each offset from the previous by $3''$, in an observing sequence for each mask, and then subtracted from each exposure to greatly reduce fringing in the red. The exposures for each slitlet were reduced separately and then co-added. One-dimensional spectra were extracted for each targeted object, as well as the occasional serendipitous source. Wavelength calibration of the 1-D spectra was obtained from arc lamp exposures taken immediately after the object exposures. A relative flux calibration was obtained from long-slit observations of the standard stars HZ44, G191B2B, and Feige 67 (Massey & Gronwall 1990).

3. Object selection and photometry

SExtractor (Bertin & Arnouts 1996) was used to find objects in the i_{775} and z_{850} images and measure their magnitudes. Threshold and deblending settings were used as in Benítez et al. (2004). Although we have extensive spectroscopy, the ACS imaging reaches considerably deeper along the cluster luminosity function. Thus, we have chosen to use colors ($i_{775} - z_{850}$) and $(J - K_s)$ to isolate a set of probable cluster members. In Fig. 2, the ($i_{775} - z_{850}$) and $(J - K_s)$ colors are shown as a function of galaxy age, using BC03 stellar population models, redshifted to $z=1.106$. Early-type cluster members would have ages of at least 0.5 Gyr, corresponding to $(i_{775} - z_{850}) > 0.8$ mag and $(J - K_s) > 1.45$ mag. At first, we give a larger color margin and select as potential cluster

members all morphologically-classified early-type galaxies with $0.5 < (i_{775} - z_{850}) < 1.2$ mag and $(J - K_s) > 1.45$ mag, down to $z_{850} = 24$ mag (the limiting magnitude of Postman et al. (2005) morphological classification, that included all clusters in our sample at redshift unity). Our results in this paper are based on this morphological classification and a detailed discussion of the uncertainties in this classification can be found in that work. This selected sample includes 38 galaxies within the ACS field.

Our final colors were measured within galaxy effective radii (R_e), to avoid biases due to galaxy internal gradients, following the approach in Blakeslee et al. (2003a) and van Dokkum et al. (1998, 2000). R_e values were derived with the program GALFIT (Peng et al. 2002), constraining the *Sersic* index $n \leq 4$ (as in Blakeslee et al. 2003a). To remove differential blurring effects (the PSF is $\sim 10\%$ broader in the z_{850} band) each galaxy image in both i_{775} and z_{850} was deconvolved using the CLEAN algorithm (Högbom et al. 1974). The $(i_{775} - z_{850})$ colors were measured on the deconvolved images within a circular aperture of radius equal to R_e , or 3 pixels, whichever is larger. Our median R_e is ≈ 5.5 pixels (≈ 13 kpc at $z=1.106$). Our final results do not change (within the uncertainties) if the effective radii are calculated via a two component (Sersic bulge + exponential disk) surface brightness decomposition technique using GIM2D (Marleau & Simard 1998; Rettura et al., in preparation), that permits us to better fit the galaxy light profile.

The photometric uncertainties due to flat fielding, PSF variations, and the pixel-to-pixel correlation for ACS (Sirianni et al. 2005) were estimated by measuring the standard deviation of photometry in the background for circular apertures in the range of the measured effective radii. These photometric errors were added in quadrature to the Poisson uncertainties in the measured fluxes for each object. The derived errors in the colors are between 0.01 and 0.03 mag down to $z_{850} = 24$ mag. SExtractor MAG_AUTO were used for the z_{850} magnitude in the color-magnitude relation; these are fairly robust, though may systematically miss a small fraction of the light (Benítez et al. 2004).

We finally color-selected 34 early-type (E, S0 and S0/a) galaxies with $0.8 < (i_{775} - z_{850}) < 1.1$ mag within $2'$ from the cluster center, taken

as the center of the X-ray emission (Stanford et al. 2002). Images of the color-selected galaxies are shown in Fig 3, Fig 4 and Fig 5. Moreover, there are late-type galaxies with luminosities that are similar to the red-sequence bright early-type galaxies (Fig. 6). Of the 34 color-selected galaxies, 15 are spectroscopically confirmed cluster members, one (S0/a, with magnitude $z_{850} = 24.2$ mag) is a confirmed non-member, and the others were not targeted for spectroscopy. The selection in $(i_{775} - z_{850})$ at $z = 1.1$ therefore appears to be robust: only one of the 16 selected galaxies with measured redshifts is a non-member. We expect few of the other 18 to be interloper field galaxies.

4. Color-Magnitude Relation

The color-magnitude relation for the final color-selected objects is shown in Fig 7. Red dots are ellipticals, orange squares and stars are S0 and S0/a galaxies, respectively. Smaller black symbols represent early-type galaxies that do not lie on the red sequence. Small triangles are late-type galaxies. Boxes are plotted around confirmed cluster members. Confirmed interlopers are circled in the figure. Surprisingly, the two brightest cluster members are not ellipticals, but S0. The brightest of these two galaxies lies ≈ 700 kpc ($\approx 1.2'$) from the cluster center, and the other bright S0 at ≈ 300 kpc ($\approx 0.6'$). Moreover, there are late-type galaxies with luminosities that are similar to the red-sequence bright early-type galaxies. Two of them lie on the red-sequence and are confirmed cluster members, at ≈ 80 kpc from the cluster center (see also below in the discussion of the color and morphology distribution as a function of distance from the cluster center).

We fitted the following linear color-magnitude relation to various subsamples of the galaxies:

$$i_{775} - z_{850} = c_0 + Slope(z_{850} - 23) \quad (1)$$

The solid line in Fig 7 is the fit to the color-magnitude relation for the ellipticals, the black dotted line is the fit to the CMR for the S0s, and the dashed-dotted line the fit to the full sample, within $2'$ from the cluster center (see discussion below). The dashed line is the fit to the full sample of early-type galaxies in RXJ1252.9-292 from Blakeslee et al. (2003a), scaled to this redshift with BC03 evolved stellar population models, with solar metallicity and a formation age of

2.6 Gyr (since Blakeslee et al. 2003a obtains elliptical mean ages > 2.6 Gyr). The long-dashed vertical line is the magnitude limit of the morphological classification $z_{850} = 24$ mag. The results for different morphological samples are given in Table 1.

A robust linear fit based on Bisquare weights (Tukey’s biweight; Press et al. (1992)) has been used to fit the color–magnitude relation. Uncertainties on the parameters were estimated by bootstrapping on 10,000 simulations. The scatter around the fit was estimated from a biweight scale estimator (Beers, Flynn & Gebhardt 1990), that is insensitive to outliers, in the same set of bootstrap simulations. The internal color scatter (σ_{int}) was measured in two ways: 1) to the scatter around the fit, we have subtracted in quadrature the average uncertainty due to the galaxy color error; and 2) we have calculated the internal scatter for which the χ^2 of the fit would be unity. Both methods give us internal scatters consistent to within a few 0.001 mag. All galaxies in this sample lie within three sigma from the fit.

The X–ray distribution appears to be very symmetric, and largely confined within $1'5$ from the cluster center. We calculated the CMR zero point and scatter within $1'$ (which corresponds to a scale of ≈ 0.5 Mpc at this redshift), and within $1'5$ (≈ 0.7 Mpc), and within $2'$ (≈ 1 Mpc, the scale used for the analysis of RXJ1252.9-292). According to the results in Table 1, the internal color scatter increases when adding populations between $1'$ and $2'$, especially for the S0 and S0/a populations, as also observed in local samples (e.g. van Dokkum et al. 1998), with only a small increase in sample size. We will therefore focus on the results obtained for color–selected galaxies within $1'$ from the cluster center (where 90% of the color–selected galaxies lie). The slope of the elliptical CMR (-0.033 ± 0.015) is slightly steeper than the observed slope in RXJ1252.9-292 (-0.020 ± 0.009), and in Coma when the latter are shifted to the observed colors at $z \sim 1.1$, using non-evolving BC03 stellar population models, but still consistent within the uncertainties. We do not find a flatter (with respect to Coma) slope as in Stanford et al. (2002). However, the S0 sample shows a much shallower slope (0.005 ± 0.023) than the ellipticals, resulting in a much flatter slope for ellipticals and S0s together (-0.024 ± 0.020). This

can explain why a shallower slope was found in that work, in which elliptical and S0s were not separated. The spectroscopically–selected elliptical plus S0 slope (-0.010 ± 0.034) is also flattened by the S0 population, while the spectroscopically–selected ellipticals have a slope (-0.021 ± 0.046) similar to that of RXJ1252.9-292 and Coma. All the difference in slope are however within the uncertainties and are statistically insignificant.

Using Bruzual & Charlot (2003; BC03) stellar population models, as in Blakeslee et al. (2003a), we derive a constraint on the age of the stellar populations in the galaxies from galaxy colors and the scatter of the CMR (van Dokkum et al. 2001; Blakeslee et al. 2003a). Two simple models have been considered and our conclusions will depend on the chosen models. The first model is a *single burst* model, in which galaxies form in single bursts at random times t_f , between the age of the cluster and the recombination epoch. The second is a model with *constant star formation* in a range of time between t_1 and t_2 , randomly chosen to be between the age of the cluster and the recombination epoch. Colors for 10,000 galaxies were simulated with their scatter around the CMR to be dependent on the burst age. In Fig 8, we show the simulated scatters as a function of burst age, with solar, half solar and twice solar metallicity model. We will assume solar metallicity in what follows. From the scatter ($\sigma_{int} = 0.042 \pm 0.010$) in the colors of the galaxies classified as ellipticals, we obtain ages > 2.1 Gyr ($z > 2$), with a mean luminosity–weighted age $\bar{t} = 3.31$ Gyr ($z_f \approx 3.1$), assuming the random single burst model. From the constant star formation model, we obtain ages > 1.6 Gyr ($z > 1.7$), with a mean luminosity–weighted age $\bar{t} = 3.26$ Gyr ($z_f \approx 3$). This agrees with the conclusion (e.g. Blakeslee et al. 2003a; Holden et al. 2004; Lidman et al. 2004; De Lucia et al. 2005) that the elliptical population in clusters of galaxies formed at $z_f > 3$, and has evolved mainly passively until $z = 1.1$.

In the (U-B)–rest frame (using BC03 stellar population models with solar metallicity and age equal to 4 Gyr), a scatter in ($i_{775} - z_{850}$) of 0.042 ± 0.010 corresponds to $0.050 + / - 0.011$. As pointed out in van Dokkum (2000) and Blakeslee et al. (2003a), CMR scatters vary little with redshift. The Blakeslee et al. (2003a) scatter for the elliptical CMR in RDCS 1252–2927 (0.024 ± 0.008),

correspond to a scatter of 0.042 ± 0.014 in the (U-B)–rest frame, indistinguishable within the uncertainties from our result.

The scatter in the CMR for galaxies classified as S0 ($\sigma_{int} = 0.044 \pm 0.020$) is comparable to the one in the E CMR, but the galaxy colors are bluer and are not compatible with a population that is as old as the ellipticals. All the S0s lie below the elliptical color–magnitude relation. In fact, between the elliptical and the S0 CMR fits there is a zero point difference of 0.07 ± 0.02 mag, with the S0s being bluer than the ellipticals. One of the three S0/a galaxies has a color that is 0.07 mag redder than the elliptical CMR, and another has a color that is ≈ 0.15 bluer than the CMR relation for Es. The inclusion of the S0/a galaxies does not significantly change the fitted CMR for the S0s.

When we consider all galaxies within $2'$ from the cluster center, the S0 and total early–type slopes are similar, while the color offset in the CMR is still present (0.05 ± 0.02 mag). The S0 population of this cluster has a very peculiar CMR with respect to the average cluster of galaxies. In fact, for several other studies the CMR of the S0 population has a similar zero point and on average a larger scatter with respect to the elliptical population (van Dokkum et al. 1998; Blakeslee et al. 2003a; Holden et al. 2004; De Lucia et al. 2004), quite different from our results. We will discuss this peculiar behavior in detail in the rest of the paper, including an examination of orientation effects on the classification.

In Fig. 9, the near-IR (Vega magnitudes) and ($i_{775} - z_{850}$) (AB magnitudes) colors are shown compared with single burst stellar population model predictions from BC03. The S0 colors are consistent with young (< 2 Gyr) solar metallicity, or older (< 3.5 Gyr), half solar metallicity populations. If the difference in E and S0 mean colors is mainly due to metallicity, then even if the two populations were formed at the same epoch, ellipticals must have been able to retain more metals than the S0s, i.e., they were more massive at a given luminosity (given the observed mass–metallicity relation for early-type galaxies, e.g., Tremonti et al. 2004, Bernardi et al. 2005, and references therein). This would imply higher mass–to–light ratios for the ellipticals with respect to the S0s. However, the lack of strong evolution in the slope and scatter of the CMR from the present out to $z \sim 1$ suggests

that the CMR is mainly the result of a metallicity–mass (i.e. metallicity–magnitude) relation (e.g., Kodama & Arimoto 1997; Kauffman & Charlot 1998 Vazdekis et al. 2001; Bernardi et al. 2005). So, at a given magnitude we do not expect large metallicity variations.

If the offset is due to a different star formation history, a model with solar metallicity and with an exponential decay of the star formation will reproduce the offset at a galaxy mean age of ≈ 3.5 Gyr. This age is consistent with the small scatter observed in the S0 CMR. We would then be observing galaxies that followed different star formation: single burst and passive evolution for the ellipticals and exponentially decaying star formation for the S0s. An exponential decay in the star formation is observed in field spiral samples (Rowan–Robinson 2001). If this is the case, our S0 population might be the evolved product of an old spiral population that was already in place in this cluster when the ellipticals formed and then gradually lost available gas for star formation.

If the E vs S0 color difference is mainly due to a difference in age, for a solar metallicity and a single burst BC03 template with age 4 Gyr, the color difference corresponds to an age difference of ~ 1 Gyr. For clusters of galaxies at $z > 1$, the cluster members on the red sequence are only a part of all the progenitors of present–day early–type galaxies. Some of today’s galaxy progenitors would have been bluer than the red sequence at these redshifts (van Dokkum & Franx 2001). In the S0 population of this cluster, we may be seeing the transitional progenitor population that in ~ 1 Gyr will evolve onto the same red sequence as now occupied by the ellipticals.

Either of the latter two scenarios would be consistent with the Postman et al. (2005) observed deficit of the S0 population of our ACS cluster sample, when compared to lower redshift samples, implying that part of the S0 population is still forming in clusters at redshifts around unity.

5. Galaxy shape properties

Since the galaxies classified as S0 in RXJ 0910+5422 are found to be systematically bluer (with respect to the red sequence) than the S0 populations observed in previous studies, we wish to examine further the properties of these

galaxies in terms of their shapes and light distributions, and how they compare to the elliptical and spiral samples in this and other clusters. The shape parameters that we will consider are Concentration and Asymmetry (Abraham et al. 1996; Conselice et al. 2004), Sersic index n , and galaxy axial ratios.

5.1. Asymmetry and Concentration

In Fig 10 (left), we compare the Asymmetry A and the Concentration C for ellipticals, S0s, and spirals with $(i_{775} - z_{850})$ colors between 0.5 and 1.2 mag. The Asymmetry parameter is obtained by subtracting a 180-degree rotated image from each original galaxy image, summing the residuals and including a correction for the background. The Concentration parameter is defined as in Abraham et al. (1996) as the sum of the galaxy flux within an aperture $r_{0.3}$ divided the total flux. $r_{0.3}$ is calculated using the SExtractor fit to the galaxies at 1.5σ above the background. The obtained semi-major and semi-minor axes from this fit were multiplied by 0.3 to derive the $r_{0.3}$ aperture (see also Homeier et al. 2005b). Early-type and late-type galaxies lie on different regions in this A vs C plane. All our red sequence S0s have $A < 0.3$ and $C > 0.3$. All but one have $A < 0.2$ and $C > 0.3$. This is the same locus in the A - C plane that is occupied by most early-type galaxies in Abraham et al. (1996) and in our Postman et al. (2005) low-redshift sample (Fig 10, right). This last sample includes 5 strong lensing clusters observed as part of our ACS GTO program [Zw1455+2232 ($z=0.258$), MS1008-1224 ($z=0.301$), MS1358+6245, CL0016+1654 ($z=0.54$), and MS J0454-0300 ($z=0.55$)]. Visual and automated classification for this cluster in the i_{775} -band for all galaxies with $i_{775} < 22.5$ was performed by Postman et al. (2005). We conclude that the S0 population presents statistical parameters typical of an early-type population (low asymmetry and high compactness).

5.2. Sersic Indices

Fig 11 plots Sersic index n as a function of galaxy effective radius R_e , both from our GALFIT modeling, for ellipticals, S0s and spirals with $(i_{775} - z_{850})$ colors between 0.5 and 1.3 mag. Red sequence ($(i_{775} - z_{850})$ color between 0.8 and 1.1 mag) galaxies are shown by large diamonds.

Most spirals have $n < 2$ and most early-types have $n > 2$, as expected. However, the n values do not permit us to discriminate between S0s and ellipticals in a unique way, unless they are combined with goodness-of-fit information for the Sersic model (e.g. the *Bumpiness* parameter introduced by Blakeslee et al. 2005)

6. Axial Ratios

6.1. Axial Ratio Distribution

In Fig 12 we compare the apparent axial ratio from SExtractor versus effective radii for elliptical and S0s with $(i_{775} - z_{850})$ colors between 0.5 and 1.3 mag. The axial ratios have been verified by using ELLIPROF (the isophotal fitting software that is used for Surface Brightness Fluctuations analysis in Tonry et al. 1997 and Mei et al. 2005) on each galaxy image, after the cleaning procedure. As above, red sequence galaxies are shown by large diamonds. The red sequence ellipticals and the bluer S0s have different axial ratio distributions, with all red sequence S0s showing axial ratios $\frac{b}{a} \lesssim 0.7$, and nearly all red sequence ellipticals with $\frac{b}{a} > 0.7$. Assuming axisymmetric disks (oblate ellipsoids) viewed with random orientation, and with a Gaussian distributed intrinsic axial ratio (with mean equal to 0.3 ± 0.1 (extreme thin disk), 0.5 ± 0.1 (early-type galaxy) and 0.75 ± 0.1 (elliptical) (Jorgensen & Franx 1994)), one would expect $\gtrsim 40\%$, $\gtrsim 60\%$, and $\gtrsim 90\%$, respectively, of the S0s to have axial ratios above 0.7. Just 9% (1 out of 11) of the red sequence S0s are observed to have an axial ratio this large (or 22% for the full S0 sample in this cluster field) (Fig 13; top). The random probability that the S0 axial ratios would show such a low fraction with $\frac{b}{a} > 0.7$ is less than 1%. This is a very simple model, but it points out a lack of round S0s, indicating either that there is some orientation bias in the classification, or that this class of objects is intrinsically prolate in shape. Jorgensen & Franx (1994) found a similar deficit of round S0s in the center of the Coma cluster. They concluded that part of the face-on S0s were classified as elliptical galaxies. Fabricant et al. (2000) also found a deficit of round S0s in the cluster CL 1358+62, at $z=0.33$. Their analysis shows that ellipticities and bulge-to-total-light-ratio do not allow us to distinguish elliptical from S0 galaxies. The other

two ACS GTO clusters at $z > 1$ (RXJ1252.9-292 and RX J0848+4452) do not show a similar lack of round S0s, as 90% of the red sequence ellipticals (out of ≈ 70) and 47% of the S0s (out of ≈ 35) have $\frac{b}{a} > 0.7$ (Fig 13; bottom). This bias is also not observed in other clusters of our ACS Intermediate Redshift Cluster Survey (see Fig 5 from Postman et al. 2005), for which more than 40% of the S0 galaxies have axial ratios above 0.7.

The observed peculiarity of the RXJ 0910+5422 S0 axial ratio distribution might call into question our result above that the S0s have a significant color offset with respect to the ellipticals. For instance, if there is a bias in our color measurement procedure which causes elongated objects to have colors that are too blue, then the color offset found above may be artificial. Such a color bias might occur if the high inclination angles bias our R_e measurements to higher values, and if the S0s become progressively bluer at larger radii. We first examine this possibility, then proceed to discuss resolutions to the peculiarity of the S0 axial ratio distribution, with the aim to establish if a misclassification of face-on S0s as ellipticals would bias the measurement of the offset between the elliptical and S0 CMR zero points.

6.1.1. Internal color gradients

It is conceivable that our $(i_{775} - z_{850})$ colors could be biased by aperture effects in the nearly edge-on S0s, for which the (possibly) bluer outer disks might contribute more to the galaxy colors than in the rounder ellipticals population. If this effect were severe enough, it might mimic the offset in color of the S0s and ellipticals found above. We test this possibility here. S0 and elliptical internal color profiles are shown in Fig 14 and Fig 15. The gradients have been calculated with aperture photometry on the same images used to calculate our $(i_{775} - z_{850})$ colors. Circles are $(i_{775} - z_{850})$ colors at different radii, the cross the $(i_{775} - z_{850})$ color at the effective radius, used for the CMR.

The S0 colors profiles do not show strong gradients. In particular, the $(i_{775} - z_{850})$ colors calculated at the effective radii are not systematically bluer than colors determined at smaller radii. Most of S0 galaxies have flat profiles; one has a blue inward gradient (ACS ID 1621; $z_{850} = 23.72$ mag, $(i_{775} - z_{850}) = 1$ mag). In two galaxies (ACS ID 1393 and 3177) the colors in the central

$0.15''^2$ are redder than the color at the effective radius. When compared with elliptical gradients, on average S0 colors do not appear biased towards higher effective radii and bluer colors than the ellipticals. We note that three elliptical galaxies show blue inward gradients (ACS ID 1753, 1519, 3323).

6.1.2. Orientation or intrinsic shape: Axial ratios vs $(i_{775} - z_{850})$ colors

Orientation biases are known to occur in the classification of ellipticals and S0s in local galaxy samples. For instance, Rix & White (1990, 1992) showed, based on both isophotal and dynamical modeling, that a large fraction of ellipticals contain a disk component with at least $\sim 20\%$ of the light, but which is hidden due to projection effects. Jorgensen & Franx (1994) found a strong deficit of round S0s in a sample of 171 galaxies in the central square degree of the nearby Coma cluster, and concluded that inclination angle played a large part in the classification of Es and S0s. Michard (1994) proposed that, except for the bright boxy ellipticals without rotational support, early-type galaxies comprise a single class of oblate rotators with orientation being the main criterion for classification as either E or S0. On the other hand, van den Bergh (1994) explained the predominance of flattened S0s by invoking two distinct subpopulations: bright disky objects intermediate between ellipticals and spirals, and a fainter population of prolate objects.

We now address the question of whether the galaxies classified as S0 in RXJ 0910+5422 are preferentially flattened in shape because of an orientation bias in the classifications or intrinsically prolate shapes. If it is an orientation bias, then this could mean either that (1) face-on S0s have been misclassified as ellipticals because their disks are not apparent, or (2) that edge-on spirals tend to be called S0s because the spiral structure is obscured. Either would result in a predominance of flattened S0s. However, in the former case, the misclassification of face-on S0s as ellipticals would tend to blur any color separation between the two classes, while in the latter case, a color offset might be introduced between the two classes because of contamination by bluer spirals. Because we do observe a color offset between galaxies classified as E and S0, with the S0s being bluer, it is possible to

look for the “missing” population of face-on blue galaxies by examining ellipticity versus color. If a population of round blue objects is found, we can then determine the nature of the classification bias, and whether it biases our color offset measurement.

Histograms of the axial ratio distributions for ellipticals and S0s are shown in the top panel of Fig. 13. We find that 60% of the early-type red sequence galaxies have $\frac{b}{a} > 0.7$, but 95% of these low-ellipticity galaxies are classified as Es. However, if we split galaxies instead by color, using $(i_{775} - z_{850}) < 0.99$ mag as the separation point, then we find that 54% of all galaxies bluer than this separation have $\frac{b}{a} > 0.7$, while 43% of the red sequence galaxies bluer than this [$0.8 < (i_{775} - z_{850}) < 0.99$ mag] have $\frac{b}{a} > 0.7$ (Fig. 16). Thus, the deficit of round S0 galaxies (which are also significantly bluer than the mean of the E class) is not found when the early-type galaxies are split based purely on color. This suggests that some of the bluer round galaxies are the face-on counterparts of those classified as S0.

Fig 17 shows axial ratios vs $(i_{775} - z_{850})$ color residuals with respect to the total early-type galaxy CMR relation, for all galaxies in the RXJ 0910+5422 red sequence. Galaxy types are coded with different symbols; using the color residuals in this way takes out the effect of the magnitude dependence of the colors. There are five round blue ellipticals, i.e., with $\frac{b}{a} > 0.7$ and on the blue side of the early-type CMR. If these are the face-on counterparts of the blue S0s, then the S0 axial ratio distribution becomes much more in line with expectations for a randomly oriented disk population (35% are rounder than $\frac{b}{a} = 0.7$). Further, we note that four other ellipticals were classified E/S0 in Postman et al. (2005); if these are also taken as face-on S0s, then the axial ratio distribution comes in very close agreement with expectations. We conclude that the face-on S0s in RXJ 0910+5422 are classified as ellipticals, just as in local early-type galaxy samples.

From our axial ratio simulations and statistics from our $z \approx 1$ ACS GT0 sample, the number of blue S0 galaxies might be between 25 and 40% higher than estimated in section 5.3.1. Moreover, the inclusion of a few blue S0s in the elliptical red-sequence will have the effect of increasing very slightly the observed CMR scatter for the ellip-

ticals. The uncertainty in the Postman et al. (2005) S0 fraction in RXJ 0910+5422 is significantly larger than 40% and hence a systematic change by this amount for one cluster does not alter any of the results or conclusions in that paper.

Throughout the paper, we continue to use elliptical and S0 classifications from Postman et al. (2005), but keeping in mind the presence of this possible projection effect.

7. Color trends, velocity dispersion and merging activity

Stanford et al. (2002) have analyzed the X-ray and near-IR properties of this cluster. This system appears to be fairly relaxed based on its regular X-ray profile; however, they find indications that the cluster is in an early phase of formation. In fact, the Chandra ACIS data show evidence for temperature structure, possibly due to an infalling group or mass streaming along a filament. The soft component of the X-ray emission (0.5–2 keV) dominates the X-ray center of the cluster, while to the south there is a harder component (2–6 keV) (see Fig. 6 from Stanford et al. 2002). The cluster does not have a central BCG or cD galaxy, and the X-ray emission center does not correspond to an optical grouping of galaxies; rather a number of luminous confirmed cluster members are linearly distributed, at least as projected on the sky (as shown in Fig 1). We do not observe any strong trend of the galaxy color $(i_{775} - z_{850})$ with distance from the cluster X-ray center (Fig. 18). Surprisingly, though not statistically significant, the bluer galaxies are concentrated toward the cluster center, instead of the outskirts, as in the other ACS intermediate redshift cluster sample (Demarco et al. 2005; Goto et al. 2005; Homeier et al. 2005; Postman et al. 2005). This tendency might support the hypothesis that we are observing sub-groups of galaxies in an edge-on sheet, e.g a group of bluer disk galaxies on a redder, older population of ellipticals.

There are 10 confirmed elliptical and 5 confirmed S0 members in the center of the cluster ($R < 500$ kpc). The average S0 redshift is 1.102 ± 0.002 and the average elliptical redshift is 1.105 ± 0.007 (the given uncertainties are standard deviations around the mean). This indicates small relative velocities (the two redshifts

are indistinguishable given the errors) between the classes and is true regardless of the possible classification bias discussed above. Unfortunately, our spectroscopic sample does not permit us to track the cluster central structure in detail. The average relative velocity between the confirmed E and S0s of ≈ 500 km/s (that also corresponds to the cluster velocity dispersion; see below) is fairly small. If merging of two distinct groups of galaxies is happening along the line of sight, we expect much higher velocity dispersions and/or relative velocities between the infalling S0s and the ellipticals.

Stanford et al. (2002) also suggest that active galaxy-galaxy merging should be observed, based on the X-ray temperature structure. To investigate any on-going dynamical activity, we calculated the cluster velocity dispersion, and the merger rate. From the 25 spectroscopically confirmed members (all galaxy types included) the line-of-sight rest-frame velocity dispersion is $\sigma = 675 \pm 190$ km/s, using the software ROSTAT from Beers, Flynn, & Gebhardt (1990). The available Chandra data give X-ray temperatures ranging from $kT = 7.2^{+2.2}_{-1.4}$ keV (Stanford et al. 2002) to $kT = 6.6^{+1.7}_{-1.3}$ keV (Ettori et al. 2004). Wu et al. (1999; see also Rosati et al. 2002) gives the relationship between kT and σ for relaxed clusters, which predicts that the velocity dispersion corresponding to the measured X-ray temperature should be ≈ 1000 km/s, considerably higher than we have found. Again, in the case of merging groups (along the line of sight) we would also have expected a higher velocity dispersion.

8. Red galaxy pairs

The quality of the ACS data allows us to discern merging activity among the cluster galaxies. If we assume that galaxy pairs with projected separations less than $20h_{70}^{-1}$ kpc are physically associated, we observe 13 associated early-type galaxies, nine galaxies of which lie on a filamentary structure about ≈ 100 kpc from the cluster center (Fig. 1). As noted above, RXJ 0910+5422 lacks any cD galaxy near the center of the X-ray emission (see also Fig. 1), but rather has a filamentary group of galaxies around the X-ray center.

The nine early-type interacting galaxies within this filamentary structure (at radius of $\sim 100h_{70}^{-1}$ kpc from the X-ray center) include 3

unique pairs (yellow arrows in Fig. 1), plus a galaxy triplet (the three components marked with red arrows in Fig. 1). Each of the 3 pairs consists of a bright elliptical with a smaller companion (all closer than $10h_{70}^{-1}$ kpc), while the triplet is a large E with two smaller S0s (also closer than $10h_{70}^{-1}$ kpc; one of these two S0s is ACS ID 1621, the S0 with an inward blue gradient). One of the pairs (the middle pair in the figure) and the two nearest galaxies in the triplet, have essentially zero relative velocity and thus are likely merger candidates. Also two of the ellipticals with blue inward gradients lie on the central filaments, and they are both small satellites of a larger galaxy.

The other two pairs, which do not lie on the filamentary structure, are at $250h_{70}^{-1}$ kpc (two E with similar size, both with weak O II emission (Stanford et al. 2002) and $300h_{70}^{-1}$ kpc (one S0/a and one E of similar size) from the X-ray center, and have relative velocities of 10,000 km/s and 2000 km/s, respectively.

The presence of the low-velocity pairs is consistent with the low velocity dispersion, and provides evidence for the on-going hierarchical growth of the cluster (e.g., van Dokkum et al. 1999). The pairing of the bright ellipticals with smaller S0s also argues against the view that we are observing a blue S0-dominated group infalling into a red cluster elliptical population, but rather complex stellar population evolution within a filamentary structure. The red-sequence S0/a confirmed members also lie within this filamentary structure.

The observations of a significant number of red galaxy pairs in a cluster at $z \sim 1$ is interesting in the context of the recent findings by van Dokkum (2005) of red galaxy interactions in $\approx 70\%$ of 86 early-type galaxies in a selected sample of nearby red galaxies from the MUSYC (Multiwavelength Survey by Yale-Chile; Gawiser et al. 2005) and the NOAO Deep Wide-Field Survey. This work concluded that most of the ellipticals in local samples were assembled by red galaxy-galaxy mergers, denominated *dry* mergers because they would involve gas-poor early-type galaxies. At higher redshift, Tran et al. (2005b) confirmed red galaxy mergers first observed by van Dokkum (1999) in MS 1054-03 at $z=0.83$. Tran et al. selected mergers as associated pairs with projected separation less than $10h_{70}^{-1}$ kpc and relative line-of-sight velocities less than 165 km/s. As in

RXJ 0910+5422, the red early-type galaxies involved in these mergers are among the brightest cluster members. Their results suggest that most early-type galaxies grew from passive red galaxy-galaxy mergers. In our sample we observe a triplet and three red galaxy pairs with projected distances less than $10h_{70}^{-1}$ kpc. Of those, the triplet and one galaxy pair show zero relative velocity. Of the two other pairs, composed of a bright and a fainter companion, redshifts are not available for the faint companions.

9. Cluster luminosity function

To obtain a deeper understanding of the RXJ 0910+5422 galaxy population, we constructed galaxy luminosity functions in the following way. We start with the original SExtractor catalog (described in Section 3). All objects with magnitudes brighter than $i_{F775W} = 21.1$ mag were considered as foreground objects. Nine of these bright objects are confirmed non-members. The remaining seven are objects that do not belong to the red sequence and whose sizes and luminosities are much larger than those of the confirmed members, in particular those of the bright red sequence galaxies; therefore they are very unlikely to be at the cluster redshift.

The contribution to the luminosity function from both foreground and background field galaxies (hereinafter, the field) has been estimated from the galaxy counts in a reference field. The control region is taken from the GOODS-S (Great Observatories Origins Deep Survey-South; Giavalisco et al. 2004) ACS field, observed in the same filter as the cluster field. Point-like objects were eliminated in a consistent way in the cluster and in the control field, by identification of the stellar locus in the diagnostic plot of the SExtractor parameters MAG_AUTO vs FLUX_RADIUS (the selected objects have FWHM equal to the PSF in the image). Cluster and control field luminosity functions were normalized to the cluster area. Both cluster and field counts were binned with a bin size of 0.5 mag. For each bin, the field counts are subtracted from the cluster counts, taking into account the extensive spectroscopic sample (more than 60% of the objects used for the LF determination brighter than M^* have measured redshifts). Known interlopers were excluded from the analy-

sis. The uncertainties in the cluster counts after subtraction of the field contribution are calculated by adding in quadrature Poissonian uncertainties.

The luminosity functions are shown in Fig 19. The filled circles with errors are the total background-corrected cluster luminosity function. We do not include errors from cosmic variance due to the choice of the background control region. The red sequence elliptical and spheroidal (S0 and S0/a) luminosity functions are shown respectively in blue and green. The red histogram is the luminosity function of all early-type galaxies with color $0.8 < (i_{775} - z_{850}) < 1.1$ mag, excluding confirmed non-members. The histogram of red sequence galaxies in RXJ1252.9-292 is shown as the dashed red line. The background contribution is very small for the early-type sample. The red arrows show the histogram values after background subtraction. The rest-frame B magnitudes are shown on the top of the plot, calculated from colors obtained from the BC03 stellar population model and templates (Sbc, Scd) from Coleman, Wu & Weedman (1980). The solid black line is a Schechter function fit to the total cluster luminosity function. It is obtained by calculating the C (Cash 1979) statistic (a maximum likelihood statistic to fit data with Poissonian errors) on a grid in the $M^* - \alpha$ plane for each combination of M^* and α : first the normalization (ϕ^*) is calculated in order to reproduce the observed number of galaxies in the observed magnitude range, then the C statistic is computed as $C = -2\sum_{i_{bin}} n_i \ln m_i - m_i - \ln n_i!$, where n_i is the observed number of galaxies in the i th bin and m_i is the number of galaxies predicted in that bin by the Schechter function with parameters M^* , α , and ϕ^* .

The combination M^*, α which minimizes the C statistic is taken as the best-fit. If the C statistic is defined as above, the 1- 2- and 3- σ confidence levels for M^* and α can be estimated from $\Delta C = 2.3, 6.17, 11.8$. We obtain $M^* = 22.6_{-0.7}^{+0.6}$ mag and $\alpha = -0.75 \pm 0.4$.

Most of the faint-end population is composed of S0 and S0/a galaxies. The two brightest galaxies in the red sequence are S0. With respect to RXJ1252.9-292, a bright population of red sequence ellipticals is missing in RXJ 0910+5422. However, the large Poissonian errors on the bright end of the cluster population prevent us from

definitively excluding the hypothesis that the two clusters could be drawn from the same parent population. Similarly, small number statistics do not permit us to study the luminosity functions of the different red and blue faint populations in this cluster.

10. Discussion and Conclusions

In this paper we have studied the color–magnitude relations of galaxies in RXJ 0910+5422 to constrain their ages and formation histories. Our results show that the color–magnitude relation for the elliptical galaxies is consistent both in slope and scatter with that of RXJ 1252.9–292 (Blakeslee et al. 2003a, Lidman et al. 2004) and recent results from Holden et al. (2004) and De Lucia et al. (2004), confirming that elliptical galaxies in galaxy clusters show a universal color–magnitude relation consistent with an old passively evolving population even at $z \sim 1$. From the color–magnitude relation of the ellipticals, we derive a mean luminosity–weighted age $\bar{t} > 3.3$ Gyr ($z_f > 3$).

We find that the S0s in RXJ 0910+5422 define a color–magnitude sequence with a scatter similar to that found for the ellipticals, but shifted bluer by 0.07 ± 0.02 mag. This is peculiar with respect to previous cluster studies, which more typically found that the S0s followed the same CMR as the ellipticals, but with somewhat larger scatter (Bower et al. 1992; Ellis et al. 1997; Stanford et al. 1997; López–Cruz et al. 2004; Stanford, Eisenhardt, & Dickinson 1998; van Dokkum et al. 2000, 2001; Blakeslee et al. 2003a; Holden et al. 2004). Only one earlier study, van Dokkum et al. (1998) found a significantly bluer S0 population. We examine this population of blue S0s in some detail, noting that there is a strong predominance of flattened systems with axial ratios $\frac{b}{a} > 0.7$, and conclude that the face-on members of the population have likely been classified as ellipticals. If so, the color offset between the two classes would become even more significant, and the true CMR scatter for the ellipticals would be slightly lower than we have estimated. This peculiarity is not observed in other clusters of our ACS Intermediate Redshift Cluster Survey, and its amplitude is smaller than the uncertainties adopted in Postman et al. (2005).

If the observed color difference between the ellipticals and S0s is mainly due to metallicity at the same age, this would imply that the redder ellipticals were able to retain more metals than the S0s, i.e., they are more massive. However, current data suggest that the CMR is mainly the result of a metallicity–mass (i.e. metallicity–magnitude) relation (e.g., Kodama & Arimoto 1997; Kauffman & Charlot 1998; Vazdekis et al. 2001; Bernardi et al. 2005). This implies that we do not expect large metallicity variations at a given magnitude. If, instead, the offset is mainly due to age, then the implied age difference would be ~ 1 Gyr for single-burst solar metallicity BC03 models. It could also result from different star formation histories, with the S0s experiencing a more extended period of star formation. A model with solar metallicity and with an exponential decay of the star formation reproduces the offset at a galaxy mean age of ≈ 3.5 Gyr.

The blue S0s may comprise a group infalling from the field onto a more evolved red cluster population, or they may be a transitional cluster population not yet evolved all the way onto the elliptical red sequence (van Dokkum & Franx 2001). Assuming passive evolution, they will reach this red sequence after about 1 Gyr. High fractions of faint blue late type galaxies were observed in substructures infalling in a main cluster (e.g. Abraham et al. 1996; Tran et al. 2005a), and proposed as the progenitors of faint S0s in clusters. The view of this cluster as a structure still in formation is supported by X–ray observations of the cluster temperature structure (Stanford et al. 2002), the lack of a cD galaxy, and its filamentary structure that suggests merging of substructures. However, we derive a small cluster velocity dispersion, unusual for merging substructures. Moreover, the blue S0s in this sample span the same luminosity range of the bright ellipticals, are distributed towards the center of the cluster, and some of the faintest ones are physically associated with brighter ellipticals belonging to the central filamentary structure. These elements would argue against the bluer S0s being a young group merging with an existing red cluster population, and support the hypothesis that we are observing a transitional blue S0 population in a cluster core that is still evolving onto the elliptical red sequence. This result is also consistent with the deficit of S0s ob-

served in our ACS cluster sample, when compared to lower redshift samples, that implies that the S0 population is not yet in place but still forming in clusters at redshifts around unity (Postman et al. 2005). Interestingly, we also observe in this cluster potential progenitors for bright S0 galaxies: four bright spirals (spectroscopically confirmed cluster members) with z_{850} brighter than 22.5 mag and ($i_{775} - z_{850}$) between 0.5 and 1.3 mag.

Red galaxy pairs are also observed. A triplet and three red galaxy pairs have projected distances less than $10h_{70}^{-1}$ kpc, and of those, the triplet and one pair show zero relative velocity. This would be the evidence of red galaxy mergers at $z \sim 1$. van Dokkum (2005) and Tran et al. (2005b) have observed mergers of red galaxies in a nearby elliptical sample and in MS 1054-03 at $z=0.83$, respectively. They suggested a scenario in which most of the early-type galaxies were formed from passive red galaxy-galaxy mergers, called *dry* mergers, because they involve gas-poor early-type galaxies.

Future papers will analyze the ages and masses of the cluster members using our optical spectroscopy along with newly obtained Spitzer IRAC imaging. A larger sample would be needed to draw firmer conclusions about the formation of S0s.

ACS was developed under NASA contract NAS 5-32865, and this research has been supported by NASA grant NAG5-7697 and by an equipment grant from Sun Microsystems, Inc. The Space Telescope Science Institute is operated by AURA Inc., under NASA contract NAS5-26555. We are grateful to K. Anderson, J. McCann, S. Busching, A. Framarini, S. Barkhouser, and T. Allen for their invaluable contributions to the ACS project at JHU. We thank W. J. McCann for the use of the FITSCUT routine for our color images. SM thanks Tadayuki Kodama for useful discussions.

REFERENCES

- Abraham, R. G., van den Bergh, S., Glazebrook, K., Ellis, R. S., Santiago, B. X.; Surma, P., Griffiths, R. E. 1996, ApJS, 107, 1
- Beers, T. C., Flynn, K., & Gebhardt, K. 1990, AJ, 100, 32
- Bell, E.F. et al. 2004, ApJ, 608, 883
- Benítez N., Ford, H. Bowens, R. et al. 2004, ApJS, 150, 1
- Bertin, E. & Arnouts, S. 1996, A&AS, 117, 393
- Bernardi, M., Sheth, R. K., Nichol, R. C., Schneider, D. P., Brinkmann, J. 2005, 129, 61
- Blakeslee, J.P., *et al.* 2003a, ApJ, 596, L143
- Blakeslee, J. P., Anderson, K. R., Meurer, G. R., Benítez, N., & Magee, D. 2003b, ASP Conf. Ser. 295: ADASS XII, 257
- Blakeslee, J.P., *et al.* 2005, ApJ, in press
- Bower, R. G., Lucey, J. R., & Ellis, R. S. 1992, MNRAS, 254, 589
- Bruzual A., G. & Charlot, S. 2003, MNRAS, 344, 1000 (BC03)
- Cash, W., 1979, ApJ, 228, 939
- Coleman, G. D., Wu, C.-C., Weedman, D. W., 1980, ApJS, 43,393
- Conselice, C.J. et al. 2004, ApJ, 600, L139
- De Lucia et al. 2004, ApJ, 610, L77
- Demarco, R., et al. 2005, A&A, 431, 381
- Ellis, R.S., Smail, I., Dressler, A., Couch, W.J., Oemler, A. Jr., Butcher, H., Sharples, R.M. 1997, ApJ, 483, 582
- Ettori, S., *et al.* 2004, 354, 111
- Fabricant, D., Franx, M., van Dokkum, P. 2000, 539, 577
- Ford, H. C. et al. 2002, Proc. SPIE, 4854, 81
- Ford, H. C. et al. 2004, astro-ph/0408165
- Gawiser, E. et al. 2005, ApJS, in press; astro-ph/0509202
- Giavalisco, M. et al., 2004, ApJ, 600, L93
- Goto, T. et al. 2005, ApJ, 621, 188
- Högbom, J. A. 1974, A&AS, 15, 417
- Hogg, D.W., et al. 2004, ApJ, 601, L29
- Holden, B.P., et al., 2004, AJ, 127, 248

- Holden, B.P., et al., 2005a, ApJ, 620, 83
- Holden, B.P., et al., 2005b, ApJ, 626, 809
- Homeier, N.L., et al. 2005, ApJ, 621, 651
- Jorgensen, I., & Franx, M. 1994, ApJ, 433, 553
- Kauffman, G. & Charlot, S. 1998, MNRAS, 294, 705
- Kodama, T. & Arimoto, N. 1997, AJ, 320, 41
- Lidman, C., Rosati, P., Demarco, R., Nonino, M., Mainieri, V., Stanford, S. A., Toft, S. 2004, A&A, 416, 829
- López-Cruz, O., Barkhouse, W. A., Yee, H. K. C. 2004, 614, 679
- Marleau, F.R. & Simard, L. 1998, ApJ, 507, 585
- Massey, P. & Gronwall, C. 1990, ApJ, 358, 344
- McIntosh, D. H., Zabludoff, A.I., Rix, H.-W., Caldwell, N. 2005, 619, 193
- Mei, S. et al. 2005, ApJ, 625, 121
- Michard, R. 1994, A&A, 288, 401
- Mullis, C.R., Rosati, P., Lamer, G., Bohringer, H., Schwobe, A., Schuecker, P., Fassbender, R. 2005, ApJ, 623, L85
- Oke, J. B., et al. 1995, PASP, 107, 375
- Peng, C. Y., Ho, L. C., Impey, C. D., & Rix, H. 2002, AJ, 124, 266
- Postman, M., et al. 2005, ApJ, 623, 721
- Press, W.H. et al. 1992, *Numerical Recipes*, Cambridge University Press, New York
- Rix, H., & White, S. D. M. 1990, ApJ, 362, 52
- Rix, H., & White, S. D. M. 1992, MNRAS, 254, 389
- Rosati, P., della Ceca, R., Norman, C., Giacconi, R. 1998, ApJ, 492, L21
- Rosati et al. 2002, ARA&A, 40, 539
- Rowan-Robinson 2001, ApJ, 549, 745
- Sirianni, M., et al. 2005, PASP, in press
- Schlegel, D. J., Finkbeiner, D. P., & Davis, M. 1998, ApJ, 500, 525
- Spergel, D.N., et al. 2003, ApJS, 148, 175
- Stanford, S. A., Eisenhardt, P. R., & Dickinson, M. 1998, ApJ, 492, 461
- Stanford, S. A., Elston, R., Eisenhardt, P.R., Spinrad, H., Stern, D., Dey, A. 1997, AJ, 114, 223
- Stanford, S. A., Holden, B., Rosati, P., Eisenhardt, P.R., Stern, D., Squires, G., Spinrad, H. 2002, AJ, 123, 619
- Tonry, J.L., Blakeslee, J.P., Ajhar, E.A. et al. 1997, ApJ, 475, 399
- Tran, K.-V., van Dokkum, P. G., Illingworth, G.D., Kelson, D., Gonzalez, A., Franx, M. 2005a, ApJ, 619, 134
- Tran, K.-V., van Dokkum, P. G., Franx, M., Illingworth, G.D., Kelson, D., Schreiber-Foerster, N.M. 2005b, ApJ, 627, L25
- Tremonti et al. 2004, ApJ, 613, 898
- van den Bergh, S. 1994, AJ, 107, 153
- van Dokkum, P. G. 2005, AJ, in press; astro-ph/0506661
- van Dokkum, P. G., Franx, M., Fabricant, D., Kelson, D. D., & Illingworth, G. D. 1999, ApJ, 520, L95
- van Dokkum, P. G., Franx, M., Kelson, D. D., Illingworth, G. D., Fisher, D., & Fabricant, D. 1998, ApJ, 500, 714
- van Dokkum, P. G., Franx, M., Fabricant, D., Illingworth, G. D., & Kelson, D. D. 2000, ApJ, 541, 95
- van Dokkum, P. G., Stanford, S. A., Holden, B. P., Eisenhardt, P. R., Dickinson, M., & Elston, R. 2001, ApJ, 552, L101
- van Dokkum, P. G. & Franx, M. 2001, ApJ, 553, 90
- Vazdekis et al. 2001, ApJ, 551, L127
- Wu et al. 1999, ApJ, 524, 22

This 2-column preprint was prepared with the AAS L^AT_EX macros v5.2.

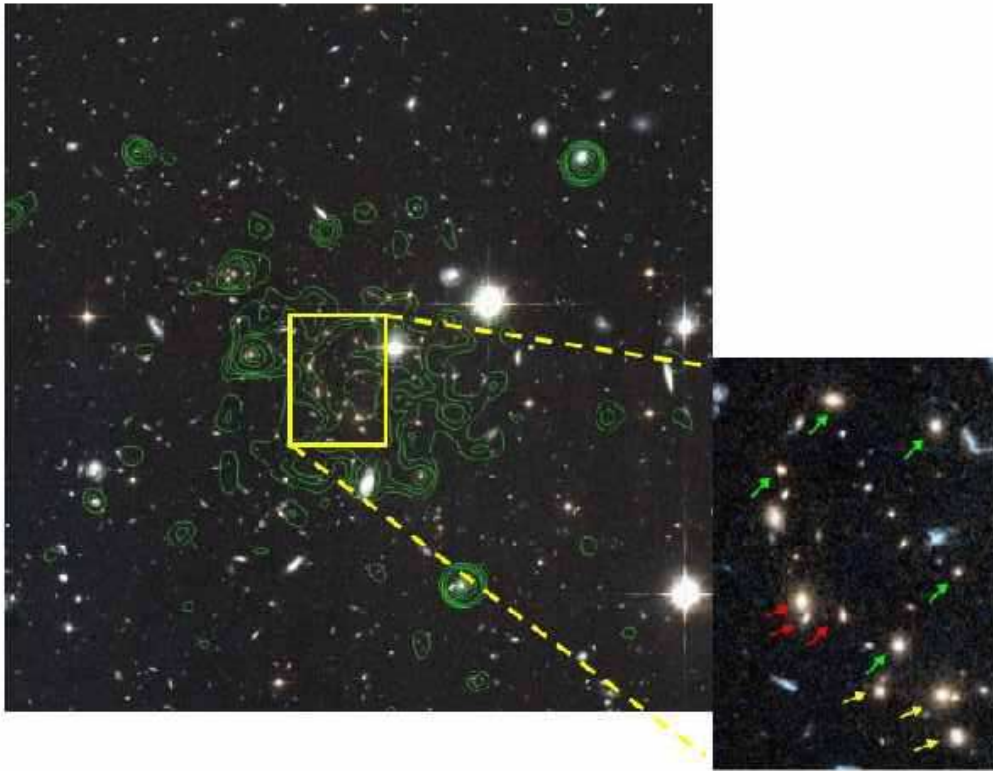


Fig. 1.— The ACS color image with X-ray contours overlaid. The X-ray observations are from Chandra ACIS-I, over the energy range of 0.5–2KeV, and were smoothed with a 5 arcsec FWHM Gaussian. North is up, East on the left. In the enlargement, galaxy pairs in the central filamentary structure are shown. Two main groups of interacting galaxies lie along the filamentary structure at the center of the cluster. The first group is shown by the yellow arrow, the second one by the red arrows. Three other red-sequence early-type galaxies are shown by the green arrows.

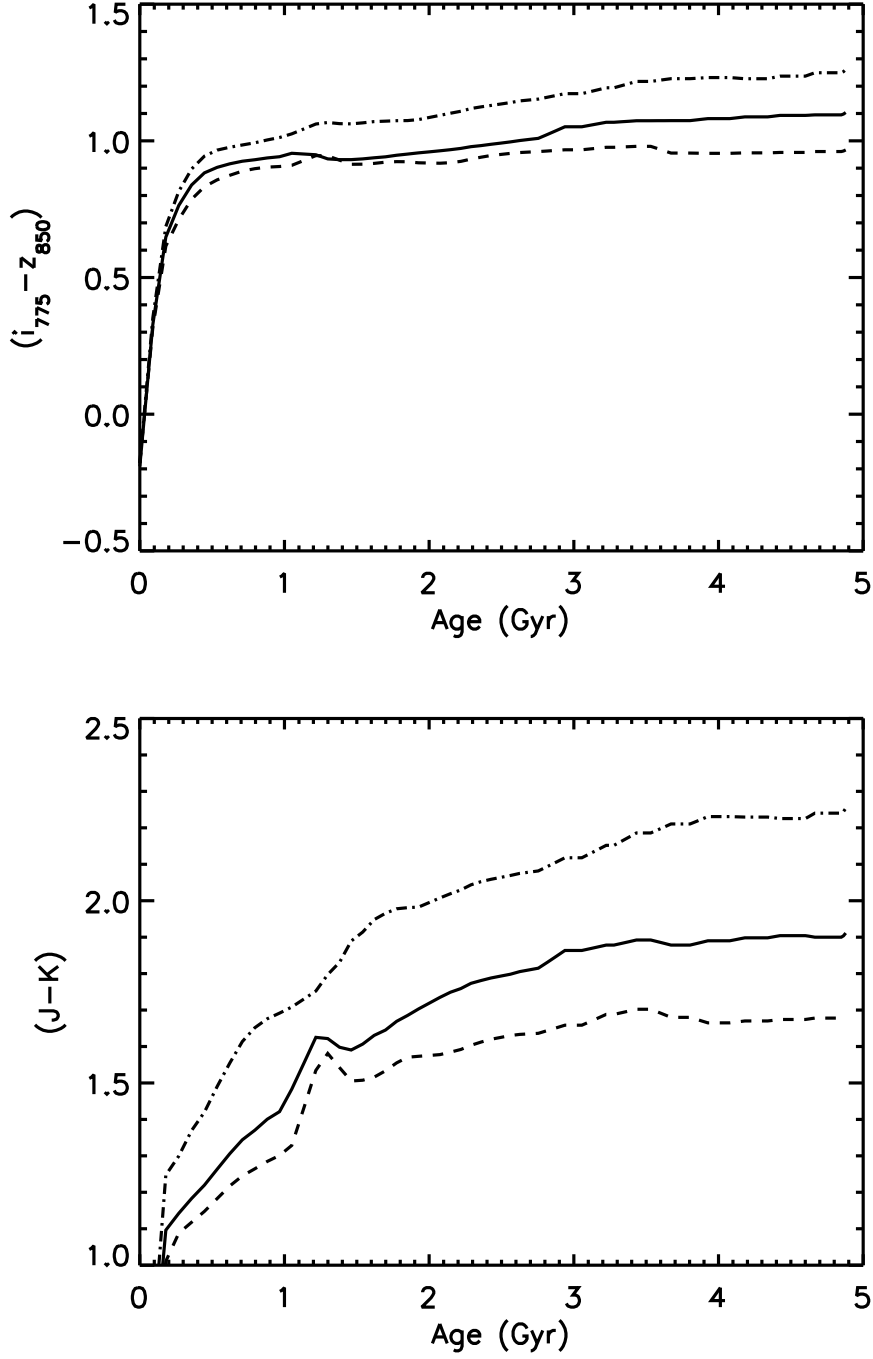


Fig. 2.— $(i_{775} - z_{850})$ and $(J-K)$ colors as a function of galaxy age. BC03 solar metallicity, age equal to 4 Gyr models are shown with a solid line. The dashed lines are for half solar and the dot-dashed lines for twice solar metallicity. We considered a sample of color-selected galaxies with $0.8 < (i_{775} - z_{850}) < 1.1$ mag and $(J - K) > 1.45$.

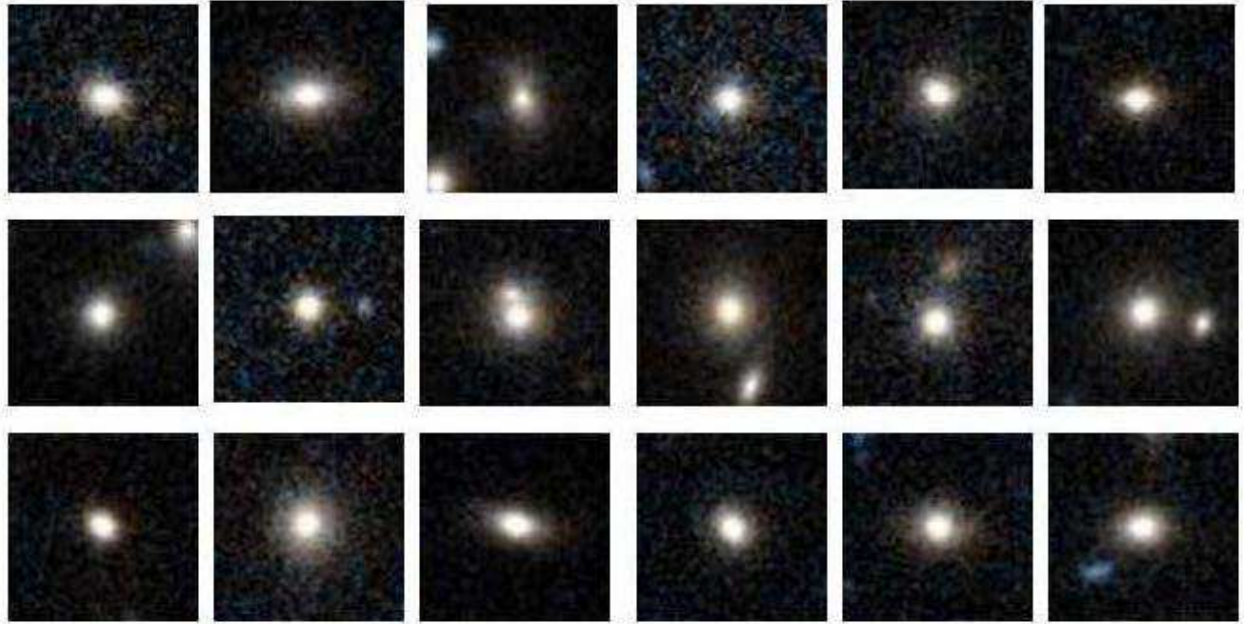


Fig. 3.— Color images of the 20 CMR ellipticals within $2'$ from the cluster center. Two of the CMR faint ellipticals, that are satellites of brighter galaxies, are shown in the same postage image of their bright companion.



Fig. 4.— Color images of the 11 CMR S0 galaxies within $2'$ from the cluster center.



Fig. 5.— Color images of the three CMR S0/a galaxies within $2'$ from the cluster center.



Fig. 6.— Color images of the four bright spirals with z_{850} brighter than 22.5 mag and $(i_{775} - z_{850})$ between 0.5 and 1.3 mag, within $2'$ from the cluster center. These spirals have luminosities that are similar to those of the red-sequence bright ellipticals.

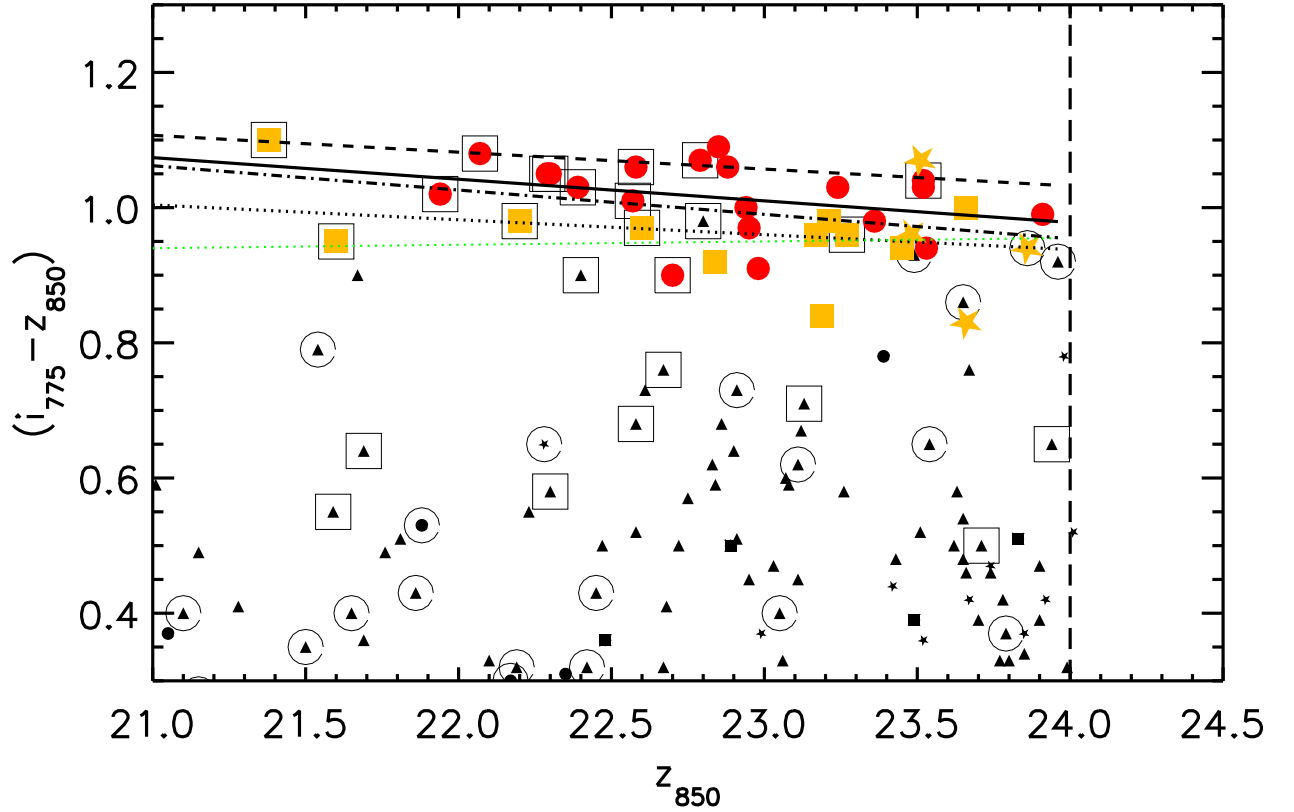


Fig. 7.— The color-magnitude relations for RXJ 0910+5422. Red circles and yellow squares are respectively E and S0 candidates on the red sequence. Yellow stars are S0/a candidates on the sequence. Smaller black circles, squares, and stars are used for the corresponding early-type galaxies that do not lie on the red sequence. Small triangles are late-type galaxies. Boxes are plotted around confirmed cluster members. Open circles are plotted around confirmed interlopers. The solid line is the fit to the ellipticals, the black dotted line the fit to the S0s, and the dashed-dotted line the fit to the entire sample within $2'$. The green dotted is fitted to the S0s within $1'$. The dashed line is the RXJ1252.9-292 color-magnitude relation scaled to the redshift and colors for RX0910+5422. The long-dashed vertical line is the magnitude limit of the morphological classification $z_{850} = 24$ mag. The S0 CMR is bluer than the elliptical CMR by 0.07 ± 0.02 mag.

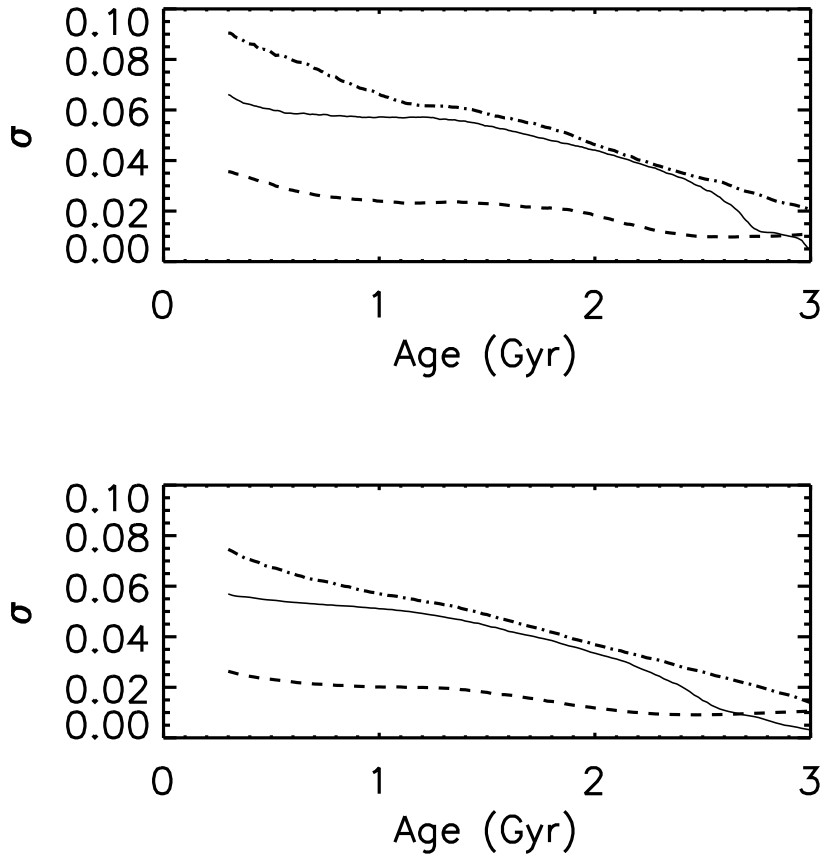


Fig. 8.— CMR scatter as a function of galaxy age from simulation obtained using BC03 single burst (on the top) and constant star formation (on the bottom) stellar population models for solar metallicity (solid line), half solar (dashed line) and twice solar (dash-dotted line). From the measured scatter it is possible to estimate the mean age of the stellar bursts.

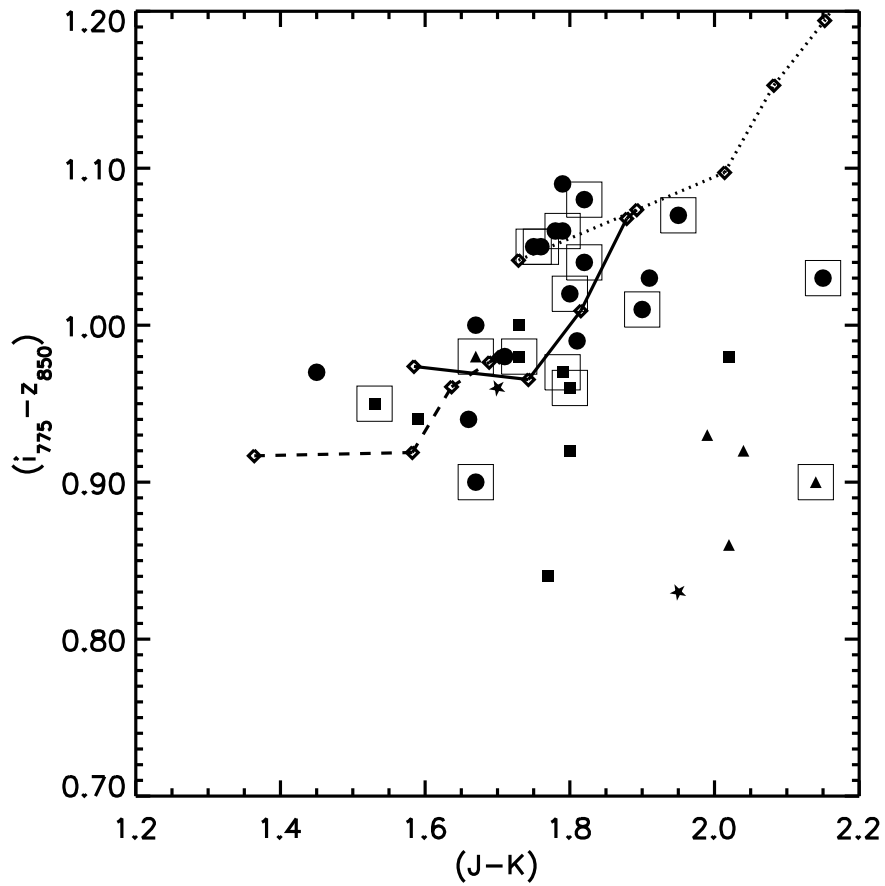


Fig. 9.— $(i_{775} - z_{850})$ (AB) vs $(J - K)$ (Vega) color. Filled circles are ellipticals, squares are S0s, and stars S0/as. BC03 single burst models are shown for half solar (dashed line), solar (solid line), and twice solar (dotted line) metallicities. Ages run from 1.5 to 3.5 Gyr, by steps of 0.5 Gyr, as diamonds from left to right. The bluer S0 colors might be due to younger ages or lower metallicities.

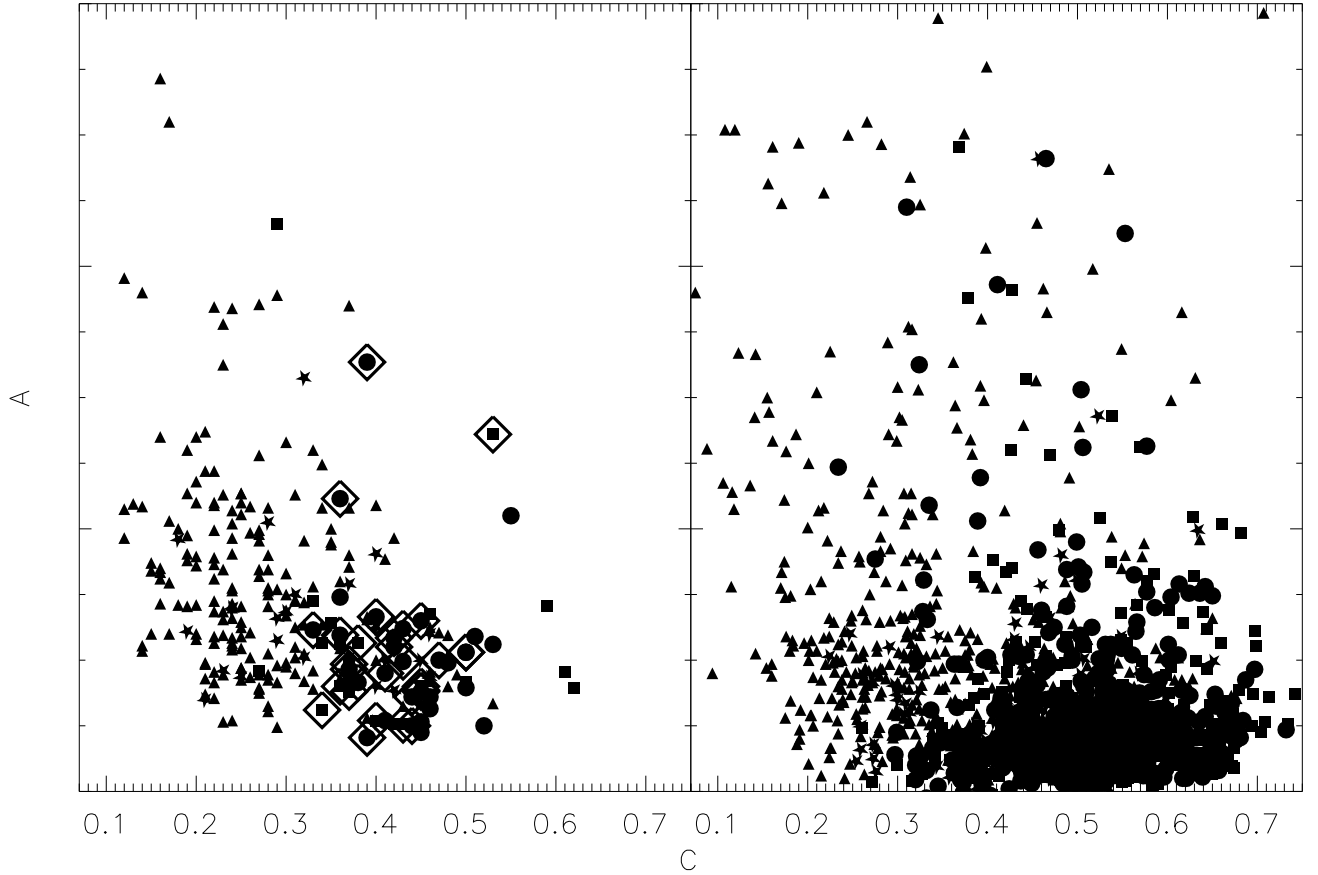


Fig. 10.— Asymmetry (A) vs Concentration (C) parameters for ellipticals (circles), S0 (squares), S0/a (stars) and spirals (triangles) in the $(i_{775} - z_{850})$ color range between 0.5 and 1.3 mag for RXJ 0910+5422 (left). Large diamonds identify red sequence $[(i_{775} - z_{850})$ color between 0.8 and 1.1 mag] early-type galaxies. On the right, the same parameters are shown for all galaxies in our low-redshift sample using the same symbols for different galaxy types. E and S0 in RXJ 0910+5422 show parameters that are characteristic of an early-type population, $A < 0.2$ and $C > 0.3$, as most of the low redshift early-type galaxies. This means that S0s were not likely misclassified late-type galaxies.

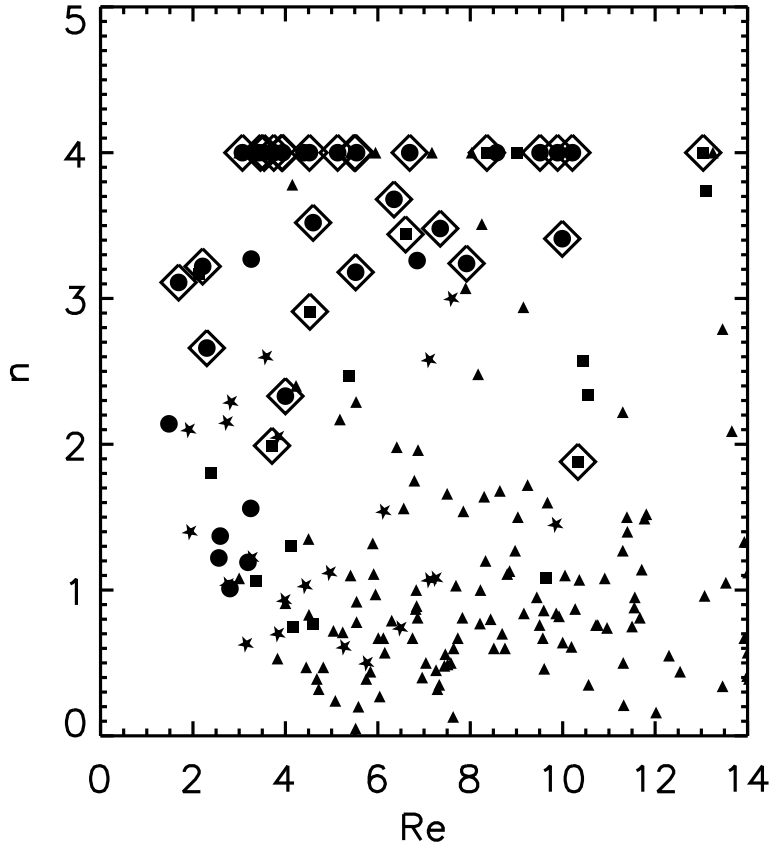


Fig. 11.— Sersic index n as a function of effective radius R_e from GALFIT is shown for ellipticals (circles), S0s (squares), S0/a (stars) and spirals (triangles) with $(i_{775} - z_{850})$ colors between 0.5 and 1.3 mag. Red sequence ($(i_{775} - z_{850})$ color between 0.8 and 1.1 mag) galaxies are shown by large diamonds. E and S0 in RXJ 0910+5422 show a Sersic index ≤ 2 . This means that S0s were not likely misclassified late-type galaxies.

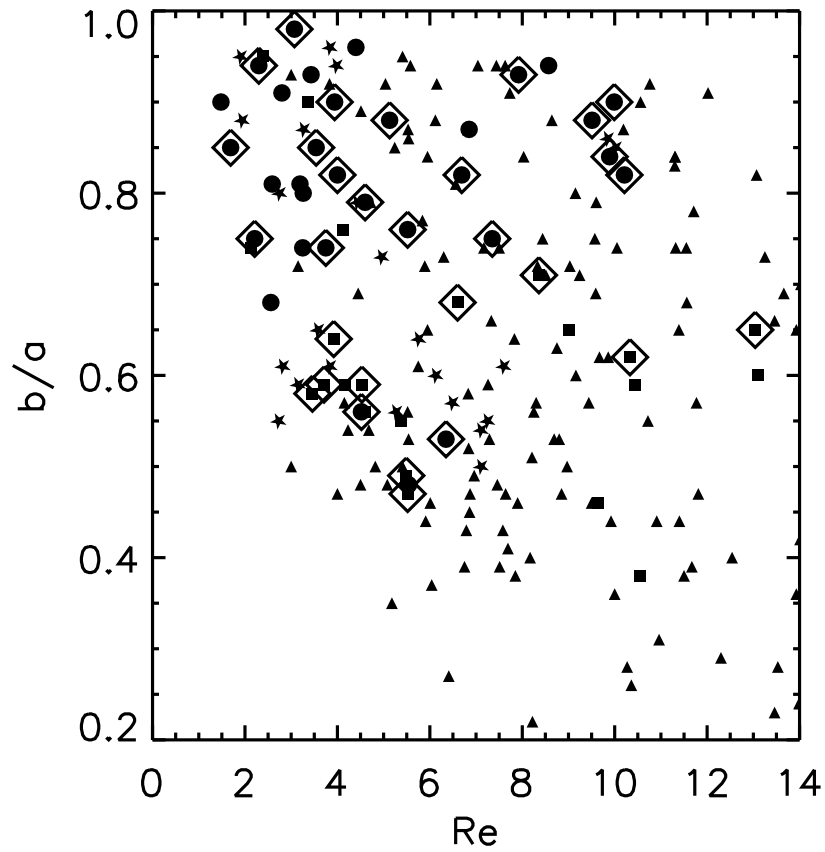


Fig. 12.— Axial ratios vs effective radii are shown for ellipticals (circles), S0 (squares) in the $((i_{775} - z_{850})$ color range between 0.5 and 1.3 mag). Large diamonds identify red sequence galaxies with $(i_{775} - z_{850})$ color between 0.8 and 1.1 mag. Stars are S0/as and triangles are spirals.

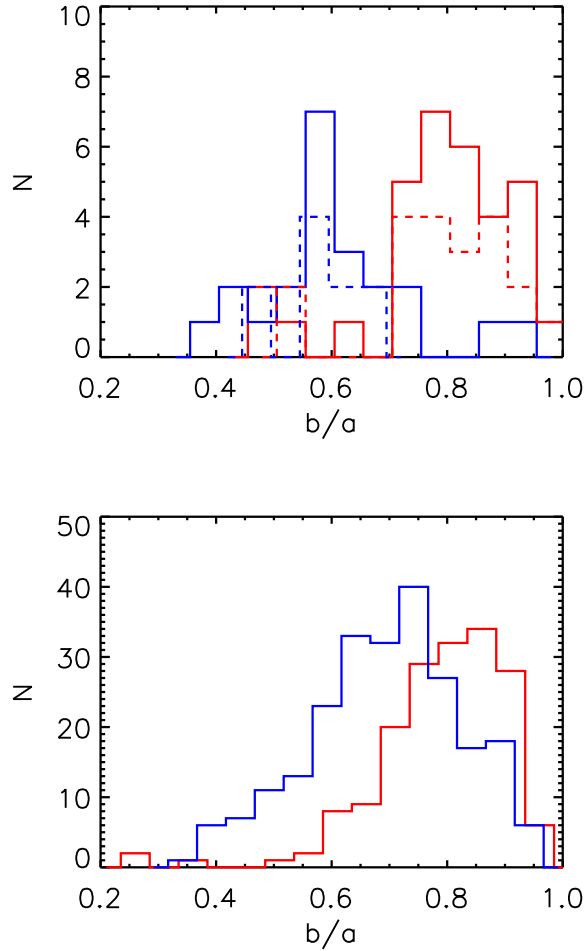


Fig. 13.— On the top, the histogram of axial ratios for the ellipticals (red line) and S0s (blue line) are shown. Dashed lines are for red sequence galaxies ($(i_{775} - z_{850})$ between 0.8 and 1.1 mag). We notice a lack of high axial ratio (low ellipticity) S0s in RXJ0910+5422. On the bottom, we show elliptical (red) and S0s (blue) distributions in RXJ1252.9-292 and RX J0848+4452. The median of their S0 distribution is consistent with that expected for nearly axisymmetric disks viewed at random inclination angles.

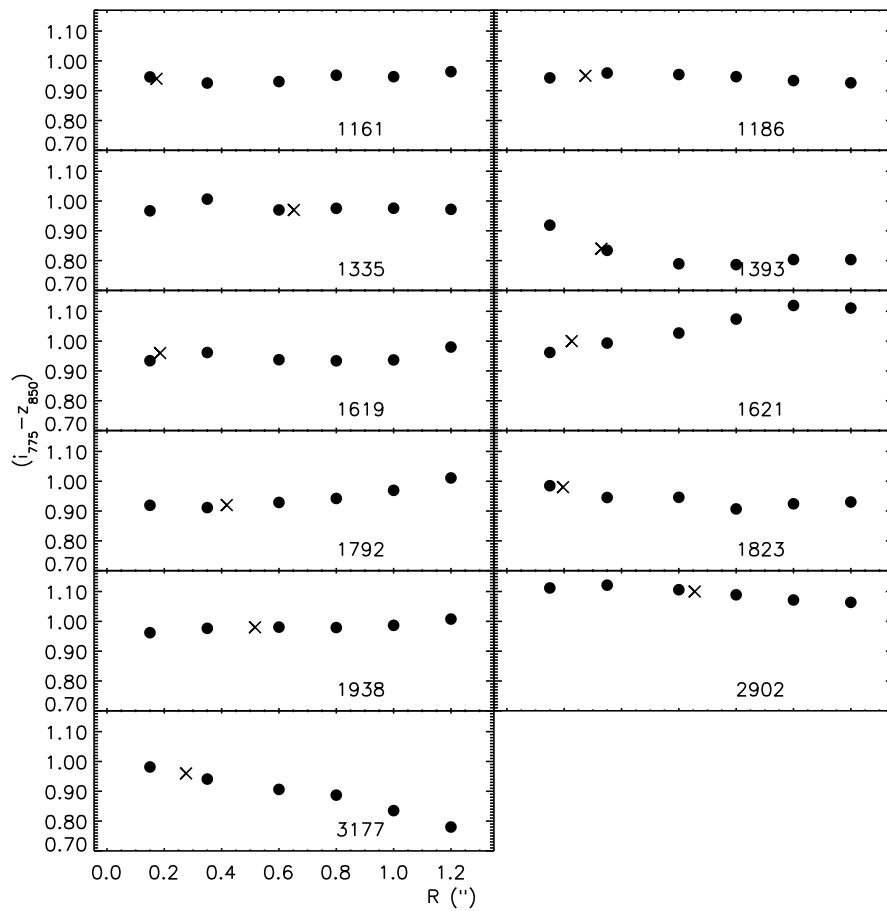


Fig. 14.— Red sequence S0 color gradients as a function of distance from the galaxy center. The cross is the color calculated at the effective radius.

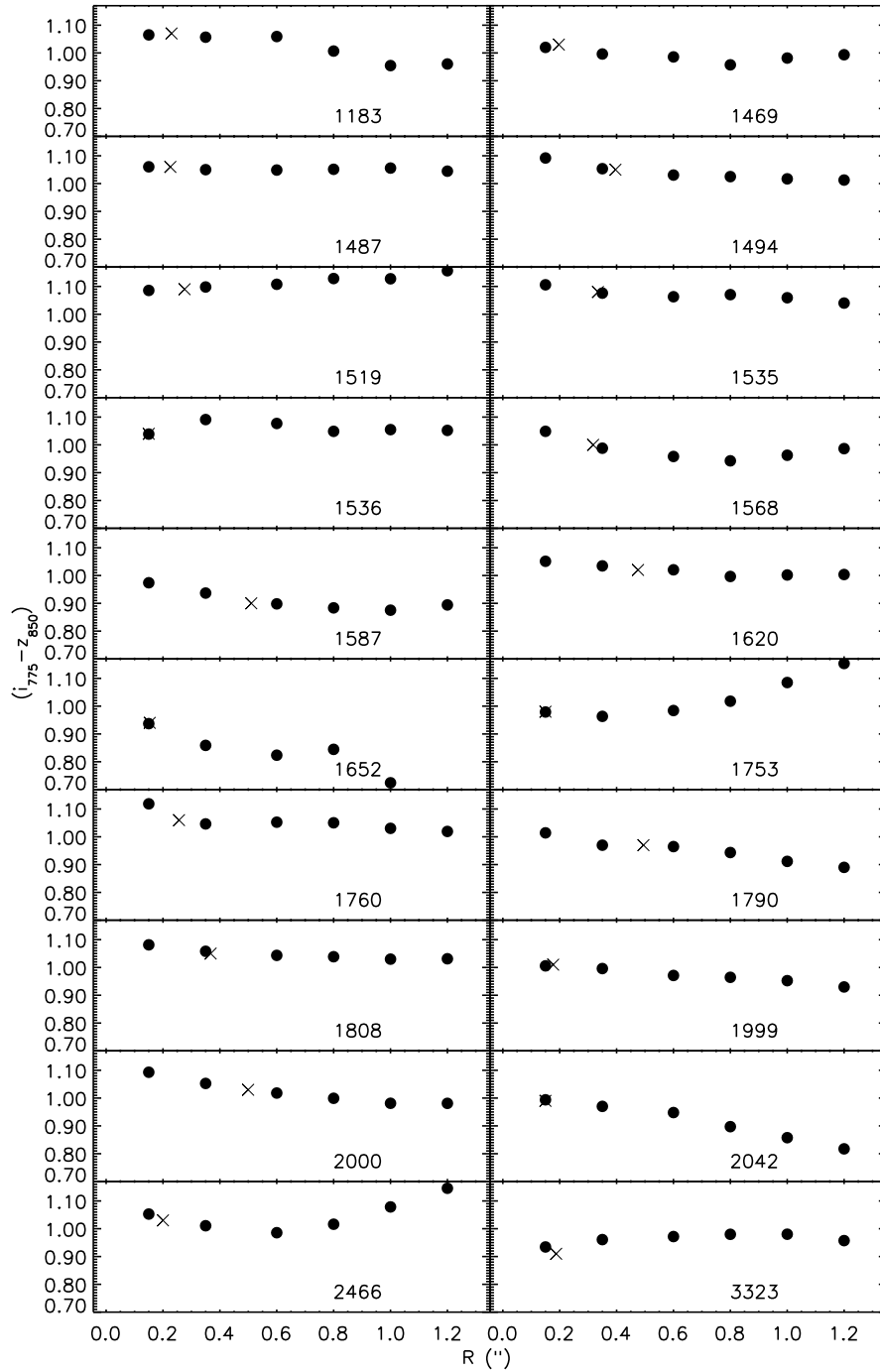


Fig. 15.— Red sequence elliptical color gradients as a function of distance from the galaxy center. The cross is the color calculated at the effective radius.

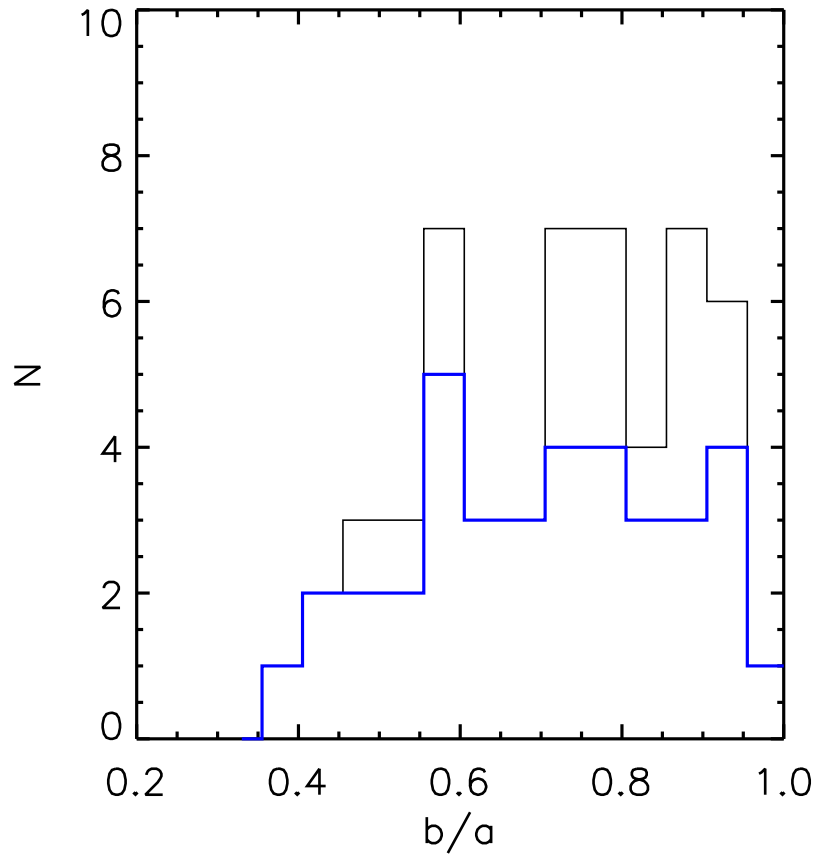


Fig. 16.— We show the histogram of the axial ratio of all early-types (black) and early-types with $(i_{775} - z_{850}) < 0.99$ mag (blue). Elliptical Whereas there is a lack of high axial ratio (low ellipticity) S0s in RXJ 0910+5422, there is no similar lack in total early-type or in the blue early-type sample.

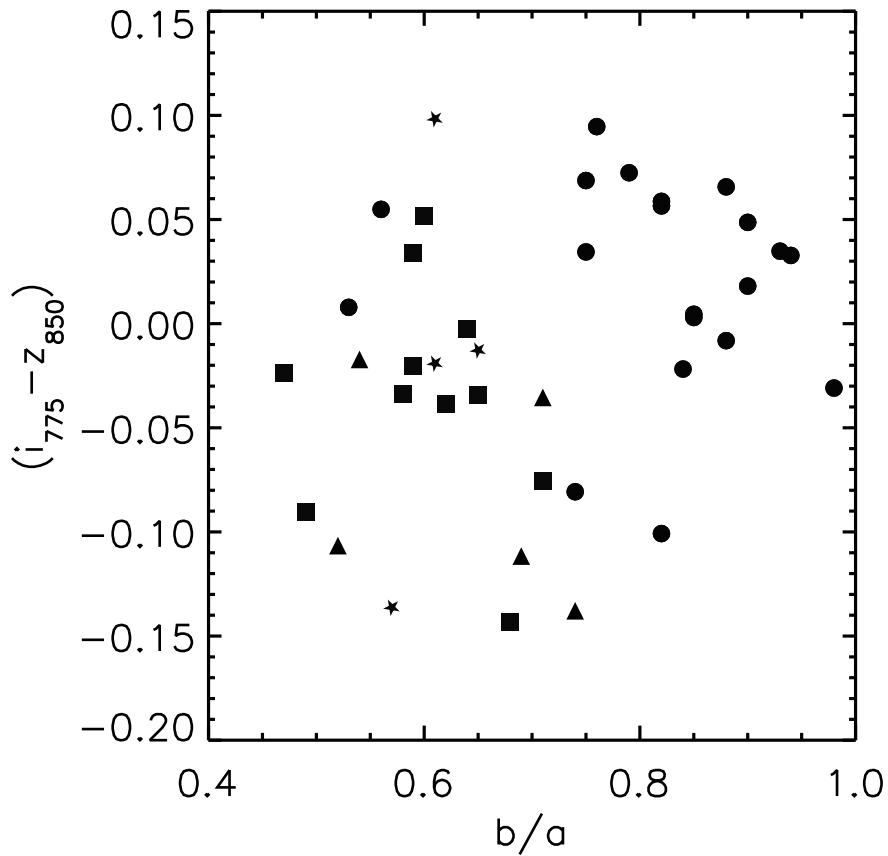


Fig. 17.— The $(i_{775} - z_{850})$ color residuals (with respect to the mean of full early-type CMR fit) is plotted versus axial ratios for red sequence ($(i_{775} - z_{850})$ color between 0.8 and 1.1 mag) ellipticals (circles), S0s (squares), S0/a (stars) and spirals (triangles). While there is a lack of S0s with $\frac{b}{a} > 0.7$, we find five ellipticals and one spiral that have blue colors (negative CMR residuals) similar to most S0s, but round shapes ($\frac{b}{a} > 0.7$), unlike the classified S0s. These may be the face-on counterparts of the elongated blue S0 population (see text).

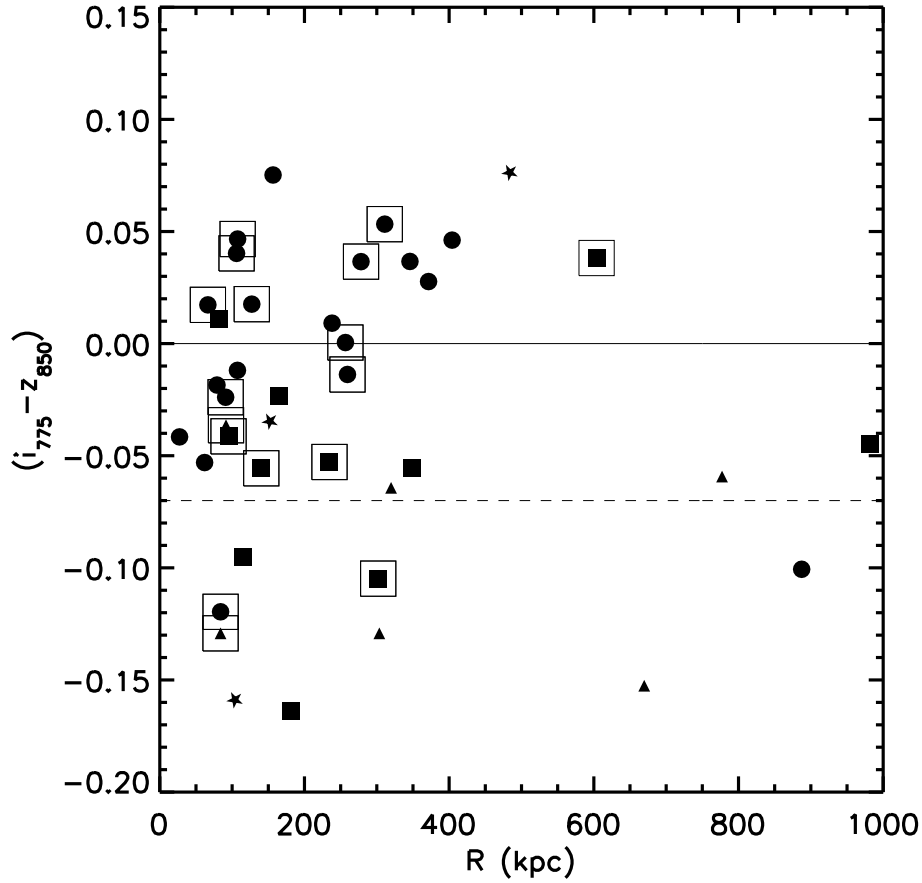


Fig. 18.— Red sequence galaxy colors, corrected by the elliptical CMR, as a function of the distance from the cluster center. Filled circles are ellipticals, squares S0s, stars S0/a, and triangles spirals. Spectroscopically confirmed members are indicated by boxes. Known non-members are omitted from the plot. The continuous and the dashed lines show the elliptical and the S0 CMR zero point, respectively. Most of the blue S0 lie close to the cluster center, not on the outskirts.

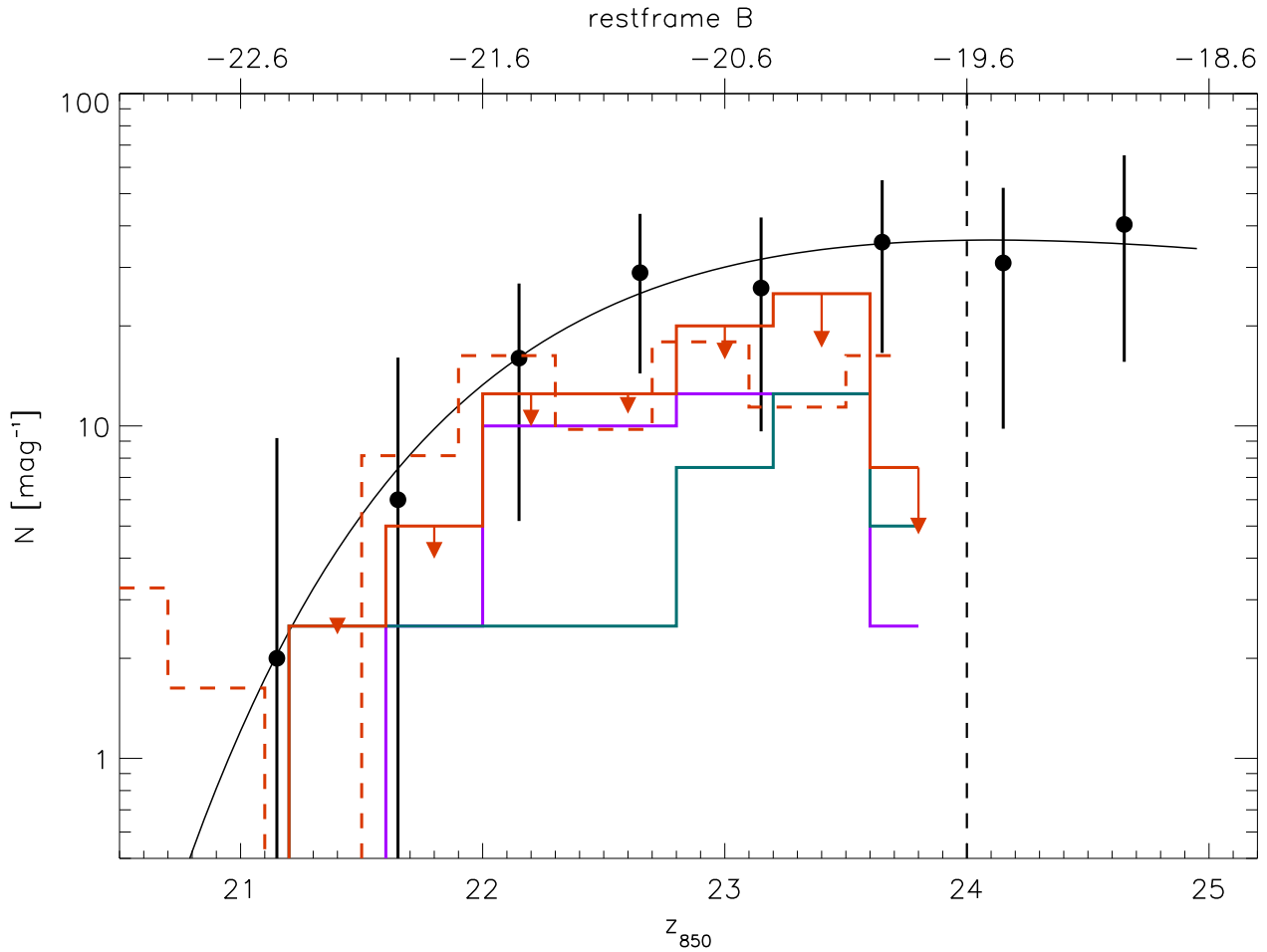


Fig. 19.— The z_{850} luminosity functions for all galaxies (black circles with errors), as well as red sequence early-type (red), elliptical (blue), and S0+S0/a (green) galaxies are shown. The faint end of the red sequence luminosity function is dominated by S0s and S0/as. The solid line is the fit to the total luminosity function. We obtain $M^* = 22.6^{+0.6}_{-0.7}$ mag and $\alpha = -0.75 \pm 0.4$. Galaxies have been classified morphologically down to $z_{850} = 24$ mag. The histogram of red sequence galaxies in RDS1252.9-292 is shown as the dashed red line, as a comparison. The red arrows show the histogram values after background subtraction.

Table 1: Color–Magnitude Relations

Sample	N	c_0 (mag)	$Slope$	σ_{int} (mag)
E+S0+S0/a ¹	31	0.99 ± 0.01	-0.030 ± 0.020	0.060 ± 0.008
E+S0 ^{1a}	14	1.00 ± 0.02	-0.010 ± 0.033	0.054 ± 0.009
E ¹	19	1.02 ± 0.01	-0.033 ± 0.015	0.042 ± 0.011
E ^{1a}	10	1.02 ± 0.04	-0.020 ± 0.044	0.047 ± 0.022
S0 ¹	9	0.95 ± 0.02	0.005 ± 0.023	0.044 ± 0.02
S0+S0/a ¹	12	0.95 ± 0.02	-0.007 ± 0.027	0.057 ± 0.015
E+S0+S0/a ²	32	0.99 ± 0.01	-0.032 ± 0.019	0.060 ± 0.008
E+S0 ^{2a}	15	0.99 ± 0.02	-0.021 ± 0.034	0.054 ± 0.009
E ²	19	1.02 ± 0.01	-0.033 ± 0.015	0.042 ± 0.011
E ^{2a}	10	1.02 ± 0.04	-0.020 ± 0.044	0.047 ± 0.022
S0 ²	10	0.95 ± 0.02	-0.012 ± 0.036	0.051 ± 0.018
S0+S0/a ²	13	0.96 ± 0.02	-0.015 ± 0.033	0.065 ± 0.015
E+S0+S0/a ³	34	0.99 ± 0.01	-0.036 ± 0.018	0.059 ± 0.008
E+S0 ^{3a}	15	0.99 ± 0.02	-0.022 ± 0.035	0.054 ± 0.009
E ³	20	1.01 ± 0.01	-0.032 ± 0.015	0.044 ± 0.010
E ^{3a}	10	1.02 ± 0.04	-0.021 ± 0.046	0.047 ± 0.022
S0 ³	11	0.96 ± 0.02	-0.022 ± 0.038	0.053 ± 0.015
S0+S0/a ³	14	0.96 ± 0.02	-0.024 ± 0.034	0.065 ± 0.013

1: within 1'

2: within 1.5'

3: within 2'

a: only confirmed members